Biotite dissolution kinetics at pH 4 and 6.5 under anaerobic conditions and the release of dissolved Fe(II)

Chemical Geology 662 (2024) 122204

Contents lists available at ScienceDirect

Chemical Geology

journal homepage: www.elsevier.com/locate/chemgeo

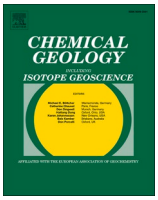

Biotite dissolution kinetics at pH 4 and 6.5 under anaerobic conditions and the release of dissolved Fe(II)

Stellan Holgersson [a,*], Henrik Drake [b], Andreas Karlsson [c], Lindsay Krall [d]

[a] Chalmers University of Technology, Department of Chemistry and Chemical Engineering, Kemivägen 4, SE-41296 Göteborg, Sweden
[b] Linneaus University, Department of Biology and Environmental Science, Hus Vita, SE-39182 Kalmar, Sweden
[c] Swedish National Museum of Natural History, Unit of Geosciences, Box 50007, SE-10405 Stockholm, Sweden
[d] Swedish Nuclear Fuel and Waste Management Company, Box 3091, SE-16903 Solna, Sweden

ARTICLE INFO

Editor: Oleg Pokrovsky

Keywords:
Biotite
Dissolution
Leaching
Fe(II)
Granitic bedrock
Anaerobic conditions

ABSTRACT

Dissolution of biotite, the main Fe-bearing mineral in granitic bedrock, is of particular importance for the remediation of reducing conditions after the ingress of oxygen, such as after mining activities or the construction of deep repositories for toxic waste. This study investigated the leaching of biotite of size fraction 0.053–0.075 mm under anaerobic conditions at room temperature and pH 4 and 6.5 for a maximum of 160 days. The changes in the concentrations of the major elements in the leaching solutions were monitored. In addition, Fe(II) was analysed separately. pH-independent rate coefficients k_{H+} were $4.8 \bullet 10^{-10}$, $6.9 \bullet 10^{-10}$, $6.3 \bullet 10^{-11}$, and $1.0 \bullet 10^{-12}$ mol^{1-n} m^{-2} s^{-1}, for Fe, Fe(II), Mn, and Si, respectively. The corresponding proton reaction orders n_{H+} were 0.61, 0.63, 0.33, and 0.09, respectively. The corresponding parameters for Al were not evaluated because of a suspected gibbsite precipitation at pH 6.5. The dissolution of biotite was found to be incongruent (non-stoichiometric) with respect to both the dissolving elements and the pH value. At pH 4, the dissolution was dominated by the octahedral layer element Fe, whereas at pH 6.5, the dissolution of the tetrahedral element Si dominated. There was no evidence of secondary phase formation, and the biotite leaching rates were consistent with those reported in previous studies conducted under aerobic conditions. In addition, the Fe(III)/Fe_{tot} ratio of biotite remained essentially unchanged before and after the experiment. This indicates that the anaerobic conditions alone have little effect on the rate and nature of biotite dissolution, although they may influence vermiculite formation. Therefore, biotite dissolution rates previously obtained under aerobic conditions may also be valid under anaerobic conditions.

1. Introduction

The potential use of bedrock as a host for the final repository of nuclear waste has been the subject of scientific research for decades. Scientific and engineering knowledge about the concept has reached the current degree of maturity, and in 2023, the concept is considered ready to be implemented for the disposal of highly radioactive spent nuclear fuel. In Sweden and Finland, repositories are to be built according to the KBS-3 concept (SKBF/KBS, 1983).

The KBS-3 concept develops an engineered repository at a depth of approximately 500 m in the granitic bedrock. Apart from engineered barriers, long-term safety also depends on the natural conditions of the site, providing tectonic stability, low groundwater mobility, additional sorption capacity of the bedrock, and reducing (anaerobic) conditions. Reducing conditions is important for preventing the oxidation of spent nuclear fuel, thereby maintaining the actinides in the fuel in a reduced and low-soluble oxidation state.

The Forsmark area in Sweden, which is the site selected for a future nuclear fuel waste repository, is dominated by a metamorphic medium-grained granite to granodiorite type, and it contains 3–12% biotite according to modal mineralogical analyses (Selnert et al., 2008) (Drake et al., 2006).

The natural reducing conditions will be reestablished after the closing of the repository by the action of Fe(II), which acts as an oxygen scavenger (White and Yee, 1985). The supply of Fe(II) to the bedrock is mainly provided by the leaching of biotite, a 2:1 phyllosilicate mineral. The 2:1 layer comprises one sheet of octahedrally coordinated cations between two sheets with tetrahedrally coordinated cations. This layer is

* Corresponding author.
E-mail address: stehol@chalmers.se (S. Holgersson).

https://doi.org/10.1016/j.chemgeo.2024.122204
Received 22 November 2023; Received in revised form 31 May 2024; Accepted 3 June 2024
Available online 5 June 2024

referred to as the TOT layer. Because every fourth tetrahedral position contains Al instead of Si, the TOT layer is negatively charged. This is balanced by the interlayer K^+ cations. The general formula for biotite is $K(Mg,Fe)_3AlSi_3O_{10}(OH,F)_2$. Three of the octahedral positions are occupied by divalent cations, making the biotite a trioctahedral mica.

Biotite is a solid solution which lies between the endmembers phlogopite $KMg_3(AlSi_3O_{10})(OH)_2$, annite $KFe_3(AlSi_3O_{10})(OH)_2$, siderophyllite $KFe_2^{2+}Al(Al_2Si_2O_{10})(OH)_2$ and eastonite $KMg_2Al(Al_2Si_2O_{10})(OH)_2$ (Rieder et al., 1998). Muscovite, which is used as an additive in some experiments in this work, is a dioctahedral mica in which only two of three octahedral sites are occupied. The ideal formula for muscovite is $KAl_2(AlSi_3O_{10})(OH)_2$.

A rigid structure is formed owing to the presence of non-hydrated K^+ in the interlayer. The bonding between different TOT layers is purely electrostatic. In acidic conditions, the ion exchange of K^+ with H^+ in biotite interlayer structure is probably the first step in the transformation of biotite into other secondary minerals. This causes an expansion of interlayer distance and a charge imbalance which is compensated with the release of octahedral cations from the sheet edges. Tetrahedral sheet Al and Si at the edges are also susceptible to proton attack but this may be a separate mechanism giving rise to incongruent dissolution of biotite, where tetrahedral and octahedral sheets dissolve at different rates (Acker and Bricker, 1992), (Malmström et al., 1996).

Interlayer expansion and clay formation have been observed with TEM (Ferrow et al., 1999), (Murakami et al., 2004). Basal plane pitting corrosion has also been observed with AFM, but only in presence of oxalic acid (Haward et al., 2011), (Cappelli et al., 2020). With oxalic acid, the overall contribution to dissolution from basal plane was found to be 10–25 lower than the contribution from edges (Cappelli et al., 2020). Thus, the incongruent dissolution is not likely to be due to a combination of basal plane and edge dissolution, but instead it is more likely due to at least two reaction mechanisms in the edge dissolution.

The leaching of biotite has frequently been studied under aerobic conditions, where Fe(II) is readily oxidised to less soluble Fe(III) (Acker and Bricker, 1992) (Kalinowski and Schweda, 1996) (Malmström and Banwart, 1997) (Bray et al., 2015) (Cappelli et al., 2020).

One anaerobic and one strongly oxidizing experiment among several aerobic at pH 4 showed that the dissolution of biotite was possibly influenced by redox conditions, however, the differences were small, which indicates that redox may not be that important for the dissolution rate (Acker and Bricker, 1992). More recent studies on biotite leaching under anaerobic conditions have primarily been conducted to explain the composition of some Precambrian paleo-sols as a result of a low-oxygen Precambrian atmosphere (Murakami et al., 2004) (Sugimori et al., 2009).

Biotite dissolution under aerobic conditions results in the formation of secondary minerals, mainly the clay mineral vermiculite, with the formula $Mg_{3-n}Fe(III)_nAl_{1.5}Si_{2.5}O_{10}(OH)_2{\cdot}4H_2O$. The mineral forms in the expanded biotite interlayer structure, and gradually transform biotite into a stratified composite, which is usually referred to as hydrobiotite (Coleman et al., 1963), (Brindley et al., 1983). Except for the replacement of K^+ with other, and hydrated, cations in the interlayer cation-exchange sites, the main biotite structure is slightly affected at this stage (Velbel, 1985).

After the dissolution of the remaining biotite structure, the hydrobiotite is completely transformed into vermiculite, which, in turn is transformed into kaolinite, $Al_2Si_2O_5(OH)_4$ (Fordham, 1990), a clay mineral which is depleted of all interstitial cations. The transformation of biotite into vermiculite involves not only the release of interlayer K^+ but also of octahedral Fe and Mg and tetrahedral Si, since it takes three molecules of biotite to form two molecules of vermiculite (Acker and Bricker, 1992). Tetrahedral Al, on the other hand, is enriched in the solid phase since the Al:Si ratio is 1:3 in biotite vs 3:5 in vermiculite.

The dissolution mechanism of biotite under anaerobic conditions is less well known but seems to follow a similar pattern. However, a major difference is that Fe(II)-rich vermiculite appears to form instead of the usual Fe(III)-rich variety (Murakami et al., 2004). Therefore, this variety may be a precursor of chlorite, which is another sheet silicate mineral which is considered an alteration mineral of primary Fe-bearing minerals (Murakami et al., 2004), (Nesse, 2000). One may therefore presume that the secondary mineral end-product may be different in aerobic vs anaerobic weathering of biotite.

The main question is, what Fe(II) concentrations are expected in granite porewater? The value of this concentration is desirable for modelling, for example, to estimate how long it will take to reestablish reducing conditions in a repository of nuclear fuel waste. However, before conducting any anaerobic leaching of granite rock, studying the anaerobic leaching of biotite is essential, which is the subject of this study.

One aim is to establish the conditions under which one can expect to reach a steady leaching rate of Fe(II) within a reasonable timeframe for the leaching experiments. Another is to provide biotite leaching rates for anaerobic conditions, which can be compared with more extensive literature data on biotite leaching under aerobic conditions. The question is whether the leaching rate and proposed reaction mechanism can be assumed to be similar for both conditions.

Therefore, in this study, a series of batch-leaching experiments were conducted under low-oxygen conditions at pH 4 and 6.5. The former pH value was chosen to attain a marked dissolution rate, whereas at the latter pH, the dissolution rate was expected to be comparatively low but more representative of natural conditions.

This study specifically investigated the potential reasons for the dissolution rate variability, such as 1) changes with time, 2) anaerobic conditions, and 3) type of leaching solution. The experiments were conducted over a relatively prolonged period (6 months) under anaerobic conditions using five types of leaching solutions. Similar experiments under aerobic conditions were not considered necessary for comparison as most literature data have been reported for aerobic conditions.

2. Theory

2.1. Mineral dissolution theory

A general empirical dissolution model for minerals is proposed (Aagaard and Helgeson, 1982), (Lasaga, 1995), (Schott and Oelkers, 1995) which is here simplified as follows:

$$rate\left(mol \bullet s^{-1}\right) = k_0 \bullet e^{-\frac{E_a}{RT}} \bullet A{\cdot}\{H^+\}^{n_{H^+}} \bullet \prod a_i^{n_i} \bullet \left(1 - e^{\frac{\Delta G_r}{RT}}\right) \quad (1)$$

where k_0 ($mol^{1-\Sigma ni}\ s^{-1}\ m^{-2}$) is the rate coefficient, $A(m^2)$ is the surface area of the mineral, and a_i (mol) is the activity of a single reactive component i with reaction order n_i. Because protons are the most common reactive components in mineral dissolution studies, the proton activity is explicitly written in Eq. (1) and the other reactive components a_i are those which are specifically involved in the proton-induced dissolution reaction. The empirical nature of Eq. (1) is usually demonstrated by giving fractional numbers of reaction order.

Corresponding expressions can be written for a mineral dissolution by hydroxide at alkaline conditions and by water molecules at neutral conditions. At the latter, all the three reactions can be regarded as competing or parallel reactions (Hermanska et al., 2022).

According to Eq. (1), the dissolution rate depends on a temperature-independent rate coefficient k_0 ($mol{\cdot}\ s^{-1}$) for the overall reaction. The coefficient is known as the pre-exponential factor in the Arrhenius equation and this times the following exponential term of Eq. (1) is simply the rate constant k (or k_{H+}) for a constant T.

According to Eq. (1), the rate also depends on the surface area $A(m^2)$ of the mineral in contact with the solution. This quantity is usually measured separately, using gas adsorption methods and by utilising the BET isotherm evaluation (Brunauer et al., 1938).

The ΔG_r (kJ mol^{-1}) is the Gibbs free energy of reaction in Eq. (1) and its inclusion follows from the requirement that the rate should go to zero as the reaction approaches equilibrium. The function is typically of a form based on the transition-state theory (Eyring, 1935). In recent studies, the notation of a chemical affinity A (kJ mol^{-1}) has been preferred instead but changes essentially nothing since the affinity is defined as:

$$A = -RTln\,(K/Q) = \Delta G_r \quad (2)$$

Where K is the equilibrium constant and Q is the activity quotient of products to reactants, which can be measured as a progress variable. From Eq. (2) it is obvious that when few products have been formed by a dissolution reaction, Q will be small and A and ΔG_r will have large negative values and the last term within the brackets in Eq. (1) will attain unity.

Usually, mineral dissolution is investigated at far from equilibrium conditions, at a constant temperature and by varying only one specific reactive component (usually {H$^+$} or {OH$^-$}) at a time. However, it has been shown that also other activities, a_i in Eq. (1), may play a role in dissolution rates, even if conditions are not close to an equilibrium.

For example, it has been found for albite (Oelkers et al., 1994) and K-feldspar (Gautier et al., 1994), that the mineral dissolution rates are faster at an excess of dissolved Si but slower at an excess of Al compared with rates where these are present in stoichiometric proportions. This means that other activities a_{ii}, besides the proton or hydroxide activities can influence the dissolution rate, even if conditions are not near any saturation, i.e. $Q << K$.

Since Eq. (1) is empirical, there have been efforts to develop theoretical models built on reaction-mechanistic approaches to explain such phenomena like the dependency of mineral dissolution also on metal concentrations at far from equilibrium conditions and the fractional reaction orders of H$^+$ and OH$^-$. Such models are presented in for example in (Oelkers, 2001) and (Crundwell, 2017). To include such models here is beyond the scope of this work, but in the future, it can be of interest to study biotite dissolution also at relatively high metal (i.e. Al, Si and Fe) concentrations.

In this work we assume that the reaction order is zero for other reactive components. Eq. (1) can then be simplified further in the specific case of studying the effect of {H$^+$} on minerals dissolution under neutral to acidic conditions, as follows:

$$rate = k_{H^+} \bullet A \cdot \{H^+\}^{n_{H^+}} \quad (3)$$

Using the surface area-normalised rates (mol m^{-2} s^{-1}), this equation can be linearised to evaluate the pH-independent rate coefficient k_{H+} (mol$^{1\text{-}nH+}$ m^{-2} s^{-1}) and the reaction order factor n_{H+} from the mineral dissolution rates measured at different pH values.

$$lognormalised\ rate = logk_{H^+} - n_{H^+} \cdot pH \quad (4)$$

Eq. (4) is only valid under acidic and neutral conditions. For alkaline conditions, a corresponding equation can be written for the rate dependency of {OH$^-$} and the corresponding parameters k_{OH-} and n_{OH-} must then be evaluated from dissolution rate data for this pH range.

2.2. Previous studies

The literature values of k_{H+} and n_{H+} for biotite dissolution at ~25 °C for the major elements (Al, Si, Fe, and Mg) are presented in Table 1. In some cases, these parameters were not stated in the source but were then deduced by fitting Eq. (4) for the given pH-dependent rates.

According to the statements in the respective study, the dissolution rates that were used here to generate the data in Table 1 were normalised with 1) the respective elemental abundance in biotite and 2) the measured BET-specific surface area A (m^2/kg).

Despite the normalisations, Table 1 shows a relative spread in the values, especially for the rate coefficients k_{H+} with three orders of magnitude difference: from 10^{-11} to 10^{-8} mol$^{1\text{-}n}$ m^{-2} s^{-1}. However, since k_{H+} is usually determined as the zero intercept of the linear dependency between two logarithmic variables (log rate and pH), this parameter is particularly sensitive to small slope shifts.

There can be other reasons for the spread of values. The rates depend on the partial area of the edges of the biotite flakes instead of the total (basal plus edge) area of the flakes (Turpault and Trotignon, 1994). According to the SEM investigations, the edge area was estimated to be 120–250 times more reactive than the biotite basal area (Turpault and Trotignon, 1994) (Bray et al., 2015). Bray et al. (2015) also suggested that the relative surface areas for the biotite sample used were 7% edge and 93% basal to the estimated geometric area. If the edge area is more reactive than the basal area, it may dominate the biotite dissolution. This is problematic if the edge area varies independently of the measured BET area, which provides variations that are not compensated

Table 1
Some selected biotite dissolution rate coefficients and reaction order factors (at ~25 °C) from the literature, based on elemental abundance and BET surface area normalised rate values. Anaerobic data in boldface.

Indicator element	k_{H+} (mol$^{1\text{-}n}$ m^{-2} s^{-1})	n_{H+}	Condition	Duration	Reference
Al	1.4(+2/−0.5)·10^{-9}	0.4 (±0.0)	CO_2-free	2 weeks	Malmström and Banwart (1997)
	2.4·10^{-8}	0.9	aerobic	<1 week	Bray et al. (2015)[b,d]
	3.2·10^{-9}	0.8	aerobic	2 months	Sugimori et al. (2009)[d]
	1.8·10^{-9}	**0.7**	**anaerobic**	2 months	Sugimori et al. (2009)[d]
Fe	2.2(+5/−1.5)·10^{-9}	0.5 (±0.0)	CO_2-free	2 weeks	Malmström and Banwart (1997)
	1.3·10^{-8}	0.8	aerobic	<1 week	Bray et al. (2015)[b,d]
	7.6·10^{-9}	0.9	aerobic	2 months	Sugimori et al. (2009)[d]
	5.7·10^{-10}	**0.5**	**anaerobic**	2 months	Sugimori et al. (2009)[d]
Mg	3.3(+7/−2.4)·10^{-9}	0.6 (±0.1)	CO_2-free	2 weeks	Malmström and Banwart (1997)
	3.5·10^{-11}	0.3	aerobic	2 weeks	Acker and Bricker (1992)[a,d]
	1.6·10^{-8}	0.8	aerobic	<1 week	Bray et al. (2015)[b,d]
	1.2·10^{-9}	0.6	aerobic	2 months	Sugimori et al. (2009)[d]
	7.7·10^{-10}	**0.6**	**anaerobic**	2 months	Sugimori et al. (2009)[d]
Si	9.9·10^{-9}	0.9	CO_2-free	2 weeks	Malmström and Banwart (1997)
	2.3·10^{-11}	0.2	aerobic	2 weeks	Acker and Bricker (1992)[a,d]
	1.5·10^{-8}	0.9	aerobic	<1 week	Bray et al. (2015)[b,d]
	6.3·10^{-10}	0.5 (±0.0)	aerobic	<3 weeks	Cappelli et al. (2020)
	8.4·10^{-10}	0.6	aerobic	2 months	Sugimori et al. (2009)[d]
	4.3·10^{-10}	**0.5**	**anaerobic**	2 months	Sugimori et al. (2009)[d]
Average[c]	3.2(+7/−3)·10^{-10}	0.6 (±0.2)	aerobic	<18 weeks	Kalinowski and Schweda (1996)

[a] Ground biotite, a calculated average of the data given for two size fractions.
[b] Open-system series, calculated average of data given for different solution matrices.
[c] Given average values based on data for several elements.
[d] Data obtained by fitting Eq.(4) to pH-dependent rates.

for by normalising with the BET area.

Furthermore, the dissolution of anisotropic minerals, such as biotite and other phyllosilicates, is suggested to be initially incongruent, even if one specifically considers only the edges, where the octahedral layer cations, Fe and Mg, dissolve faster than the tetrahedral layer cations, Al and Si (Nagy, 1995). However, according to the collected data in Table 1, the rates evaluated from octahedral elements Fe and Mg were not much faster than the corresponding rates from tetrahedral elements Al and Si. This suggests that this may not be the main cause of the large variations in biotite dissolution rates between the different studies in Table 1.

Another reason could be that the experiments were not conducted for a sufficiently long time to avoid effects from artefacts, such as those from the rapid dissolution of any fine particles initially present. This artefact usually manifests as a more rapid initial dissolution rate, which then decays to a slower rate as the fine particles dissolve (Velbel, 1985). Another type of artefact may be the effects of interference with the ion exchange reactions of the mineral itself or precipitation of secondary mineral phases. If the dissolving elements from the primary mineral phase participate in such reactions, the apparent dissolution rate will decrease.

Previous studies have focused on aerobic dissolution of biotite, and to the best of our knowledge, only one reference (Sugimori et al., 2009) presents the pH dependency of biotite dissolution rates under anaerobic conditions . The evaluated data for the dissolution rate coefficients k_{H+} for Si and Al did not deviate significantly from the corresponding anaerobic data (Table 1), but k_{H+} based on Fe seemed to be almost one order of magnitude less for anaerobic conditions than for aerobic conditions.

The fact that laboratory dissolution rates of phyllosilicates are faster than natural in-situ weathering rates is of concern when modelling natural systems using laboratory data. Several literature review studies have discussed possible reasons for this discrepancy (Nagy, 1995), (White and Brantley, 2003), (Hermanska et al., 2022).

Previously, an empirical model for estimating the dissolution and weathering rates of some common silicate minerals, including biotite, over a very wide time interval (0–10^7 years) has been presented (White and Brantley, 2003). The model is based on numerous literature data for both laboratory experiments at pH 3–7 and field studies on silicate mineral weathering. The model is essentially a parabolic expression of the area-normalised rate R (mol m^{-2} s^{-1}):

$$R = a \bullet t^{-b} \tag{5}$$

The fitted parameters for biotite are $a = 10^{-12.32}$ and $b = -0.603$ (White and Brantley, 2003).

A peculiarity of utilising a parabolic equation is that the rate R will gradually decrease over time but will never reach a final value. The parabolic rate equation typically indicates a diffusion-limited reaction (Stumm and Morgan, 1996).

In this study, a slightly different approach was adopted because the ambition was restricted to model laboratory data only and not any field data. This simplifies the modelling task because laboratory data are usually obtained under controlled and well-defined conditions. In contrast, field data probably depend on much more complex processes, many of which are only presumed to occur but can be difficult to verify.

2.3. Model for biotite dissolution

In the modelling of dissolution, the central idea employed here is that the mineral sample comprises two types of particles: the main fraction and fine particles. The assumption is that most of the particle size fractions used were covered with fine particles, despite the efforts made to clean them. This led to the assumption that the dissolution of the two particle types were controlled by different dissolution kinetics. The dissolution of the main fraction is controlled by normal first-order kinetics with respect to the surface area of the mineral reactant, as shown in Eq. (3), whereas the area of the fine particles is controlled by a first-order reaction with respect to their surface area, implying that the particle surface area A changes with time as follows:

$$-dA/dt = \lambda \bullet A \tag{6}$$

where λ(s^{-1}) is the decay constant of the fine particle surface area and is a characteristic of the fine particles and the leaching conditions (in this case mainly pH). The larger the area the faster it will diminish, when the area is approaching zero the dissolution rate of particle fines will also approach zero. The value of λ can be expected to be larger the lower the pH is. Therefore, the equation, used in this study to describe the time evolution of dissolution rate R under short-term laboratory conditions, is as follows:

$$\mathrm{R} = R_0 \bullet e^{-\lambda \bullet t} + R_\infty \tag{7}$$

where R_0 and R_∞ (mol m^{-2} s^{-1}) are the initial and final dissolution rates, representing fine particles and the main fraction, respectively. Notably, Eqs. (7) and (5) (White and Brantley, 2003) are only valid at a fixed pH, or any other reactant concentration, and describe the time evolution of the dissolution rate at this fixed reactant concentration. For the pH-independent parameters k_{H+} and n_{H+}, Eq. (4) was used, but with the rates obtained from Eq. (7) at the fixed pH values.

When evaluating the mineral dissolution rates from laboratory experiments, the concentrations of typical dissolution indicator elements (usually Fe, Si, and Al) were measured with time. To utilise the time-dependent concentration data, the rates R_0 and R_∞ were evaluated by integrating Eq. (7) with respect to time, to obtain:

$$C_t = C_0 + \frac{R_0}{\lambda} \bullet \left(1 - e^{-\lambda t}\right) + R_\infty \bullet t \tag{8}$$

The time-dependent concentration C_t used for the evaluation was corrected with the starting or background concentration $C_{0,}$ which was measured separately, and the values presented and evaluated below were, therefore, C_t-C_0.

3. Materials and methods

3.1. Biotite mineral specimen

The biotite specimen used in this study was obtained from a granitic pegmatite in Risör, Norway. The muscovite specimen originated from a granitic pegmatite within the area of Iveland, Norway and was used in some of the leaching series to simulate the presence of other minerals in granite and by its own dissolution to provide additional background elements to the leaching water. Muscovite was chosen as a presumably iron-free mineral (which in fact it was not, according to the analyses).

The chemical compositions of the minerals were analysed by ALS Scandinavia AB company, Luleå, Sweden using method TC-3 for total metal content (32 elements) in soil, sludge, sediment, and HNO_3/HCl/HF digestion and fusion. The results of these analyses are presented in Table 2. The biotite sample was characterized for Fe(II) content using Mössbauer spectrometry (see Results section). based on these analyses, the chemical formula for biotite was calculated as:

$$\mathrm{K_{1.05}\left(Mg_{0.70}Mn_{0.06}Ti_{0.18}Fe(II)_{1.81}Fe(III)_{0.25}\right)\ Al_{1.28}Si_{2.62}O_{10}(OH)_2}.$$

The density of the biotite was determined to be 3.10 kg/L, using the water displacement method (Dubois, 2011).

3.2. Mineral pre-treatment, specific surface area, and porosity analysis

In a previous study (Dubois, 2011), the biotite specimen was crushed and sieved into a 53–75 μm size fraction. The mineral was crushed using an agate pestle and mortar and then sieved using stainless-steel sieves. The size fractions were washed several times with ethanol to remove as

Table 2
Composition of biotite and muscovite. In (ppm) or boldface values (%) of dry weight.

	Biotite	Muscovite
Al	**7.08%**	**17.7%**
As	<3	<3
Ba	470	1220
Be	1.27	11.2
Ca	<100	<100
Cd	0.0996	<0.05
Co	32.8	3.74
Cr	<10	<10
Cu	17.6	3.78
Fe	**23.5%**	**11.8%**
Hg	<0.05	0.167
K	**8.4%**	**9.2%**
Mg	**3.4%**	**0.47%**
Mn	6890	50.9
Mo	<0.5	<0.5
Na	996	6340
Nb	81.8	17.1
Ni	4.97	4.46
P	<50	<50
Pb	7.74	51
S	385	<100
Sb	<0.05	<0.05
Sc	23.7	15.1
Si	**15.1%**	**19.5%**
Sn	3.68	42.7
Sr	<2	77.5
Ti	**1.76%**	**0.17%**
V	61.3	18.4
W	<1	24.3
Y	0.662	0.779
Zn	1060	68.4
Zr	23.2	11.3
Drying loss (105 °C)	0.4%	0.2%
LOI 1000 °C	0.13%	4.49%

much of the fine particulate dust as possible.

After drying the size fraction at low pressure at room temperature for several days, the specific surface area (SSA) (m^2/g) was measured on four biotite samples with a Kr gas adsorption instrument (ASAP2020, Micromeritics), taking ten points of readings of adsorbed gas in the relative pressure range of 0–0.2. The adsorption data was evaluated according to the BET isotherm (Brunauer et al., 1938) to present, together with the weight of sample, values for SSA.

The specific pore volume (SPV) (mL/kg) was measured for the four biotite samples using the same instrument but with N_2 gas. Therefore, the adsorption of gas over the entire pressure range (up to the saturation pressure) was used. Because the traditional method, using the Kelvin equation to calculate the radius of the condensate meniscus to deduce the total porosity, is reported to systematically overestimate the pore area (i.e. to be larger than the measured BET area), a method based on Density Functional Theory (DFT) was used instead, according to recommendations (Thommes et al., 2015). A DFT calculation algorithm with parameters for oxides and cylindrical pores incorporated into the instrument software was used to calculate the SPV from the gas adsorption data.

3.3. Leaching solutions

To compare the influence of different background components from a typical granitic bedrock groundwater, for the dissolution experiment five different leaching solutions were used: 1) ultra-pure water (18.2 MΩ cm, <5 ppb TOC, Milli-Q Advantage system, Merck), 2) a mixed K/Mg Cl solution, 3) same, with additional salts of Na_2CO_3, $CaSO_4$, $CaCl_2$ and NaCl, 4) a mixed K/Mg Cl solution previously contacted for several months with muscovite and 5) same as 4), but a muscovite particle was present also in the dissolution experiment with biotite. The muscovite-contacted solutions were used as simulants of granitic pore-water.

The designations used in subsequent sections and the main compositions of the five leaching solutions are listed in Table 3.

The specific recipe for the water designated FMW was based on data from an analysis of groundwater from a deep borehole at the Forsmark site, Sweden (SKB designation KFM02A 509-516 m) (Byegård et al., 2006). The salts and amounts weighed for the FMW are listed in Table 4. For the other waters containing only K, Mg, and Cl, the amounts of KCl and $MgCl_2$ were used.

The salts used were KCl (Merck, Suprapur), NaCl (Merck, Suprapur), $MgCl_2{\cdot}6H_2O$ (Aldrich 99.995%), $NaCO_3$ (Aldrich, 99.999%), $CaSO_4$ (Aldrich, 99.99%), and $CaCl_2{\cdot}4H_2O$ (Merck, Suprapur). In addition, the pH of the solutions was set to two different values, 4 and 6.5, for each water type, yielding in total ten different leaching solutions. The pH values were buffered to pH 4 with 5 mM piperazine-N,N, bis-(2-propanesulfonic acid), di-sodium salt (PIPPS, CAS 108321–07-9, Chemos GmbH) and to pH 6.5 with a 5 mM addition of N,N,N,N-Tetraethyl ethylenediamine (TEEN, CAS 150–77-6, Aldrich 98%). Note that for PIPPS, 10 mM Na was added to all pH 4 solutions. These buffers are recommended for being inert with respect to any metal complexing capacity (Yu et al., 1997).

After the dissolution of the salts and buffers, the individual solutions were adjusted to pH 4 or 6.5 with a pH meter (pHM240, Radiometer), a reference/glass electrode (pHC 3006–9, Radiometer/Hach), and either 1 M NaOH or 1 M HCl standard solutions (Titrisol, Merck) for pH adjustment. Finally, the solutions were degassed in the antechamber of a N_2-filled glovebox (O_2 < 1 ppm, UNILab, MBraun) for two to three days at 0.5 bar. The pH of the leachates was measured after the completion of the biotite dissolution experiments.

3.4. Biotite dissolution experiments

All experiments were conducted in a N_2-filled glovebox (O_2 < 1 ppm, UNILab, MBraun) equipped with a continuously operating O_2 scavenging system.

The experiments were designed as triplicate batch experiments, each with 0.05 g biotite suspended in 20 mL liquid volume, giving an S:L ratio of 1:400. There were two considerations made for choosing this ratio: 1) to fill up vessels to minimize headspace and gas volume, 2) to use minimal mass of biotite to avoid an excessive pH buffering from the solid phase. The 20 mL vessels used were of the headspace type (2009 0873, Genetec) made of glass with septa and aluminium caps (not in contact with the solution). Sampling was done with 10 mL capacity syringes equipped with a metal needle (Omnifix, Braun). Sampling of 10 mL of the leaching solution was performed on four occasions during approximately 180 days at progressively extended intervals. This means that half of the volume was sampled and replaced with a fresh leaching solution. Thus, the leaching experiments were considered semi-static; that is, the leaching solution was replaced with a fresh solution only partly and intermittently.

The headspace vial, as a vessel for the anaerobic leaching experiments, was specifically selected to minimize the gas volume in each batch. When the small gas volume equilibrates with a subsequent increase in the Fe(II) concentration in the solution from the dissolution of biotite, any residual oxygen will be rapidly consumed, and it will then potentially give even lower O_2 levels than the glove-box atmosphere.

Table 3
Designations and specifications of the five different types of leaching solution and their components.

Solution Type	Composition
0 W	water
KMW	water + K, Mg, Cl
FMW	water + K, Mg, Na, Ca, Cl, CO_3, SO_4
MEW	water + K, Mg, Cl, muscovite-contacted
MSW	water + K, Mg, Cl, muscovite solid particle included in batch

Table 4
Amounts (g) of salts weighed for preparation of 1 L simulated groundwater (FMW), based on the analyses (in mM) of a sampling of deep borehole water from Forsmark, Sweden (SKB designation KFM02A 509–516 m)*.

	K (mM)	Mg (mM)	Na (mM)	Ca (mM)	*total cations (mM)*	Cl (mM)	CO_3 (mM)	SO_4 (mM)	*total anions (mM)*	Amount (g)
Analysed*	0.85	9.54	92.2	23.3	159	145	2.07	5.31	158	
Salts										
KCl	0.85					0.85				0.063
NaCl			88.1			88.1				5.147
$MgCl_2{\cdot}6H_2O$		9.54				19.1				1.939
Na_2CO_3			4.1				2.07			0.219
$CaSO_4$				5.31				5.31		0.723
$CaCl_2{\cdot}4H_2O$				18.0		36.0				3.293

* (Byegård et al., 2006).

A flow reactor system may be a more common method for mineral dissolution studies, and was used, for example, in the anaerobic biotite dissolution study by (Sugimori et al., 2009). However, in this present study it was desirable to minimize the gas volume in contact with leaching solution and thereby enhance the anaerobic conditions over what is normally achievable with the glove-box system only (~ 1 ppm O_2). Unfortunately, only glass vials of the required head-space type were available; therefore, blank experiments were conducted to compensate for the glass leaching.

In addition to these blanks, prepared Fe(II) blanks were also used to check the stability of Fe(II) for an eventual air ingress event into the vial/glove-box system. These were made up to 2 ppm Fe(II) from a stock solution of Fe(II) (see Fe(II) analysis below) with the corresponding water (0 W, KMW, FMW, MEW, and MSW, each at pH 4 or 6.5). However, the stock solution is acidic (0.75 M H_2SO_4), and consequently resulted in a measured pH of 2.5 in these blanks, but the pH was not adjusted further. The time it takes for 10% (i.e. clearly detectable with the Fe(II) analysis method used) oxidation of Fe(II) in solution at pH 7 in air ($pO_2 = 0.2$) was calculated to $1.25{\cdot}10^{-2}$ min according to the rate equation given by (Stumm and Morgan, 1996). According to same reference, the corresponding rate at pH 2.5 is 5 orders of magnitude slower, that is 1250 min (= 20 h). Since the sampling of solutions were made at intervals of weeks to months, it was expected that any oxidation of Fe(II) due to air ingress event into vial/glovebox would be evident in the Fe(II) blanks, even if not adjusted to pH 4 or 6.5.

3.5. Elemental analyses of solutions

The concentrations of the three major elements in the biotite (Al, Fe, and Si) and one trace element (Mn) were analysed in the leaching solution samples using ICP-MS (iCAP Q, Thermo). Subsamples of 1 mL from the 10 mL samples were used for these analyses. To sample the leaching solutions with biotite, a 1 mL syringe (BD Plastipak) with a filter disc (0.45 μm, Puradisc 13, Whatman) was used to prevent sampling of biotite particles. The subsamples were then diluted, typically to 5 mL, with 0.5 M HCl (Suprapur, Merck, provided in a plastic bottle). Four different standard series of 0, 1, 5, 10, 50, 100, 500, and 5000 ppb analytes were made from 10 ppm (CPA Chem) or 1000 ppm (Inorganic Ventures) certified standard solutions. For these series, blank solutions (either 0 W, KMW, FMW, or MEW) were added to the respective standard series to obtain the same ratio of blank solution to acid as that in the samples. This was done to compensate for the presence of background salts in the water, which may affect the instrument signal when analyzing solutions with high salt contents. Furthermore, instrument drift during each analysis was followed and compensated for by the addition of an internal standard of 2 ppb Sc to both samples and standards.

The "electrolyte" elements Ca, K, Mg, Na and S concentrations were analysed in the leaching solution samples with an ICP-OES instrument (iCAP Pro XP Duo, Thermo). Subsamples (0.5 mL) from the 10 mL samples were used for these analyses. For leaching solutions with biotite a 1 mL syringe (BD Plastipak) with filter disc (0.45 μm, Puradisc 13, Whatman) was used to prevent sampling of biotite particles. The subsamples were then diluted to 10 mL with 0.5 M HNO_3 (Suprapur, Merck, provided in a glass bottle). A standard series, of 0, 5, 10 and 20 ppm analytes, was made from 1000 ppm (Inorganic Ventures) certified standard solutions. For these samples, blank matching of standards was not considered to be necessary since the sample loading was only 5% (compared to 20–30% for ICP-MS). Instrument drift during each analysis was monitored and compensated for by the addition of 2 ppm Y to both samples and standards.

The Fe(II) concentrations in the leaching solutions and Fe(II) blanks were analysed using a UV/VIS spectrophotometer (UV-1800, Shimadzu). The phenanthroline method was used (Lipps, 2022) where Fe (II) is bound into a metal complex with phenanthroline at pH 3.2, which produces a solution of intense orange colour and absorbance at 510 nm. The stated interferences of the method included other divalent metals, such as Co, Cu, and Ni > 2–5 ppm. The phenanthroline solution was prepared by dissolving 0.1 g 1,10-phenantroline monohydrate (CAS 66–71-7, 99%, Janssen) and one drop of concentrated HCl (Suprapur, Merck) in Milli-Q water, and then diluted to 100 mL. The acetate buffer solution was prepared by dissolving 25 g of NH_4CH_3COOH (99.999%, Aldrich) in Milli-Q water; to this was added 70 mL of concentrated acetic acid (99.7%, Sigma-Aldrich,), and then diluted to 100 mL.

Subsamples of 2 mL were drawn with a 10 mL syringe (Omnifix, Braun) and filtrated (0.45 μm Chromasil 25, Machery-Nagel) directly into plastic cuvettes (type 759,005, Brand) and then 0.8 mL of phenantroline solution and 0.4 mL of acetate buffer solution were added. The solution absorbance at 510 nm was measured within 1 h after the addition. Standards of 1, 5, 10 and 20 ppm Fe(II) were prepared from a 200 ppm stock solution of Fe(II). The latter was prepared by dissolving 1.404 g Fe(II) $(NH_4)_2(SO_4)_2{\cdot}6\ H_2O$ (p.A., Janssen) and 20 mL concentrated H_2SO_4 (96%, Merck) in Milli-Q water and filled up to 1 L.

3.6. Additional solid phase analyses

The biotite samples were analysed before and after the dissolution experiments using Mössbauer spectroscopy, Field-Emission Scanning Electron Microscopy (FE-SEM), Transmission Electron Microscopy (TEM) and X-ray Diffraction (XRD). These studies were conducted at the Department of Geosciences, Swedish National Museum of Natural History (Mössbauer, FE-SEM, and XRD) and Lund University (additional FE-SEM on polished sections and TEM). Only samples of biotite leached with 0 W and KMW were collected, dried, and analysed.

3.6.1. Mössbauer spectroscopy

Two biotite samples were analysed using Mössbauer spectroscopy before and after the leaching experiments. These samples were leached with KMW at pH 4 and 0 W at pH 6.5, respectively. The ground powder was mixed with thermoplastic resin and pressed into a 13 mm tablet. The spectroscopy employed a conventional spectrometer system operated in constant-acceleration mode with a ^{57}Co γ-radiation source

(nominally 1.8 GBq). The spectra were collected in 54.7° geometry at 25 °C during periods of 4 (KMW at pH 4) and 3 days (0 W at pH 6.5), respectively, each over 1024 channels covering the velocity range − 4.2 to +4.2 mm/s. Spectrum calibration was performed against Fe foil, and analysis was carried out assuming Lorentzian line shapes using the MossA program (Prescher et al., 2012).

3.6.2. Field-emission scanning electron microscopy (FE-SEM)

Small fragments of the biotite samples from the 0 W and KMW leaching experiments were analysed as loose grains before and after treatment. An environmental SEM with an FE gun (QUANTA FEG 650, Thermo Fisher Scientific) fitted with an EDS detector (Oxford X-Max 80 mm^2, Oxford Instruments) was used. The analyses were performed in a low vacuum to minimize surface charging effects. Peak and elemental analyses were performed using the Aztec software and normalised to 100 wt%. Element mapping was performed using the Aztec software. In the next step, the grains were embedded in an epoxy mount (1 in.), polished to reveal a cross-section, and analysed using a variable pressure high-resolution Schottky FE-SEM (Mira3, Tescan) equipped with an EDS (Oxford Instruments).

3.6.3. Transmission electron microscopy (TEM)

Both pristine and reacted biotite were analysed using a JEOL 3000F, 300 kV TEM at the nCHREM Centre for Analyses and Synthesis, Lund University, Sweden. The samples were divided finely with mortar and pestle and dispersed in ethanol. The particles were then collected on the instrument grid with the excess removed by filter paper.

3.6.4. X-ray diffraction (XRD)

Two biotite samples were analysed before and after the dissolution experiment. The two samples analysed after the leaching experiments were leached with KMW-type leaching water at pH 4 and 0 W-type leaching water at pH 6.5. The samples were ground in acetone using an agate mortar. The samples were placed on a background-free silicon sample holder. X-ray powder diffraction data were recorded in a powder diffractometer system using Cu $K_{\alpha 1}$-radiation (X'Pert^3, Malvern Panalytical), operated at 40 mA and 45 kV. The data were collected between 5 and 70 2θ° for 1 h with a strip detector (X'Celerator, Malvern Panalytical) to validate if there were any other minerals present. Background, peak search, and search-and-match operations were performed using HighScorePlus (4.6) software (Malvern Panalytical), and the peak positions were corrected against an external Si (metal) standard (NBS640b). The mineral phases were matched against known mineral references from the Inorganic Crystal Structure and Crystallography Open databases.

4. Results and discussion

4.1. Results of gas adsorption analyses of biotite

The results for SSA and SPV of biotite samples of size fraction (53–75 μm) are shown in Table 5.

The only significant difference between the leached and fresh biotite samples was the reduced SSA. This finding supports a dissolution model which attributes initial dissolution to the presence of fine particles, which add to SSA but very little to porosity in the main size fraction. The larger errors for post-leached biotite data were probably due to the averaging results for four biotite samples from different leaching water types because of the small amount of material available.

Table 5
Results for Specific Surface Area (SSA) and Specific Pore Volume (SPV) measurements of crushed and sieved biotite, size fraction 53–75 μm. Averages of four samples.

	Before leaching	After leaching
SSA (m^2/g)	1.59 ± 0.21	0.87 ± 0.39
Area of pores (m^2/g)	0.50 ± 0.36	0.49 ± 0.49
SPV (mL/kg)	2.57 ± 0.43	2.03 ± 1.30
porosity	0.80 ± 0.13%	0.63 ± 0.40%

4.2. Results of XRD analyses

The powder XRD data for an untreated biotite sample and samples leached with KMW at pH 4 and 0 W at pH 6.5, respectively, are shown in Fig. 1. The data experienced an enormous preferential orientation; therefore, the basal reflections of [001] and [003] were overestimated, but they matched well with the reference biotite pattern COD:96–9,002,312 (Redhammer et al., 2000). There were no signs of any other crystalline phase in either sample. In conclusion, the leached samples consisted of biotite to at least 99% since typical detection limit of XRD is 1%.

4.3. Results of Mössbauer spectroscopy

The Mössbauer spectra were fitted to two doublets, each corresponding to Fe^{2+} and two doublets corresponding to Fe^{3+} (Dyar and Burns, 1986) and the results are shown in Table 6.

The two samples were notably similar, but the Fe(III)/Fe(II) ratio was possibly enhanced in the sample leached at pH 4 compared to the sample leached at pH 6.5. The $Fe(III)/Fe_{tot}$ of the samples that had undergone treatment exceeded (KMW at pH 4) or were lower (0 W at pH 6.5) than the untreated sample by +0.9 and − 0.5%, respectively. However, these very small differences may represent the natural heterogeneity of the material and were not necessarily redox-related alterations during the experiment. Therefore, the results only indicated that a change have occurred. A previous study on experimentally weathered biotite at pH 4 under aerobic conditions showed a more significant change in $Fe(III)/Fe_{tot}$ from 17.57% for the pristine material to 19.28%, or + 1.7% (Ferrow et al., 1999).

4.4. Results of FE-SEM analyses

In the first set of FE-SEM investigations of loose grains, or flakes, some slight differences were observed in the degree of alteration between the treated and untreated batches of biotite, indicated with arrows in (Fig. 2). The leached sample show somewhat more rugged grain edges in Fig. 2b, compared to the mostly smooth grain edges for the pristine sample in Fig. 2a.

To better visualise any intragrain alteration features, FE-SEM images, line scans, and elemental maps were constructed for individual polished grain interiors. These grains exhibited very small signs of alteration. The grains showed some dissolution features (Fig. 3), but overall, they showed small elemental changes in transects over the full grains, including these dissolution features. The line scans showed some variation in chemistry, but there was mainly an increase in Cl and C at the grain rims owing to epoxy inclusion in the analysis. There was a simultaneous decrease in other elements. The alteration was indicated in several samples, both in the group of samples #1–6 (KMW leaching conditions) and #7–12 (0 W leaching conditions). Additional images are presented in Appendix A.

4.5. Results of TEM analyses

The results of the TEM analysis are shown in Fig. 4 below. No major differences were observed between the pristine and leached samples, but there was indication of an opening of the layer structure at edge in a leached sample (arrow in Fig. 4b).

The mean thickness for one TOT layer was measured in some selected cut sections of the respective TEM pictures and were found to be 9.254 Å (pristine) and 9.755 Å (leached), respectively.

A previous study of biotite weathered at pH 4 under aerobic

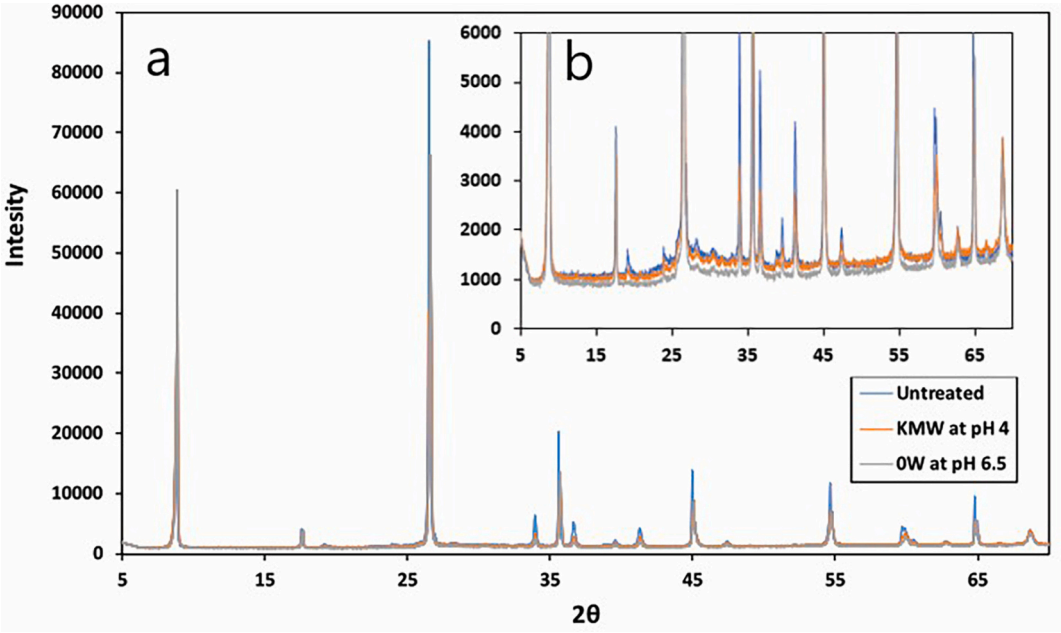

Fig. 1. a) XRD spectra biotite, untreated and leached with KMW at pH 4 and 0 W at pH 6.5 for approximately 150 d in anaerobic conditions. b) (insert) enlarged section of a).

Table 6
Results of the Mössbauer spectroscopy analyses of the Fe oxidation state of two biotite samples leached with solutions KMW at pH 4 and 0 W at pH 6.5, respectively.

	Untreated			KMW at pH 4			0 W at pH 6.5		
Assignment	CS[a]	QS[b]	Int %	CS[a]	QS[b]	Int %	CS[a]	QS[b]	Int%
Fe^{2+} I	1.127	2.579	38.06	1.132	2.568	38.09	1.127	2.577	30.93
Fe^{2+} II	1.115	2.193	49.85	1.114	2.203	48.87	1.12	2.224	57.41
Fe^{3+} I	0.464	0.478	7.93	0.447	0.533	10.69	0.462	0.47	5.38
Fe^{3+} II	0.461	0.989	4.16	0.368	1.235	2.35	0.442	0.937	6.28
Total Fe^{2+}			87.91%			86.96%			88.34%
Total Fe^{3+}			12.09%			13.04%			11.61%

[a] CS = centroid shift.
[b] QS = quadrupole splitting.

conditions for 54 days confirmed that the alteration products within the biotite structure were few and barely visible with TEM (Ferrow et al., 1999).

4.6. Results of analyses of background electrolyte elements

The results of the measurements of the background electrolyte element concentrations, presented as averages over the entire experimental period and the final pH values, are shown in Appendix E.

Most of the elemental concentrations of the electrolyte elements were stable during the entire leaching experimental period; therefore, only the average values for the four sampling occasions are shown. As expected, with the pH-buffered solutions, the measured final pH values showed only a very slight drift from the initially set values of pH 4 and 6.5.

4.7. Results analyses of dissolution products in leaching solutions

The results in this section are presented as the accumulated concentrations of dissolution products, which means that the primary data are corrected for 1) blank and 2) losses due to previous sample outtake. The primary concentrations as measured are presented in Appendix B, Tables B-1 to B-5, while the accumulated concentration values are shown in Appendix C, Table C-1 to C-5.

4.7.1. Results of Al analyses

The Al concentration data for pH 4 showed the expected initial rapid increase with time and then levelled out to a lower increase. All data series for pH 4 were successfully modelled by fitting Eq. (8). All data for pH 4 are shown in Fig. 5.

All the Al concentration values were lower for pH 6.5 (not shown), which was expected, but there was no accumulation of Al in the solution, and in some cases, negative accumulated concentrations (shown as <DL in Table C-1) were obtained. This was probably caused by the saturation of the leaching solution with gibbsite, $Al(OH)_3$ (s), which was reported to precipitate in a similar study (Acker and Bricker, 1992). Gibbsite has a $pK_s = 34$, corresponding to a solubility at a neutral pH of $2{\cdot}10^{-7}$ M (May et al., 1979), a value that agrees well with the measured initial Al concentrations for the pH 6.5 series in Table B-1. As the Al concentration was probably restricted by gibbsite at pH 6.5, this dataset was not modelled. It should also be noted that the solubility of gibbsite at pH 4 is well above 0.1 mM.

The fitted model parameters at pH 4 are presented in Appendix D and Table D-1.

The fitted R_∞ values were relatively similar for all series at pH 4, except for the MSW series (solid muscovite present), in which the final rate was slower, whereas the initial rate R_0 was faster than that of the other series. This could be due to the direct contribution from muscovite, which led to a higher Al concentration than that of the other series. A comparison of literature values for muscovite and biotite dissolution

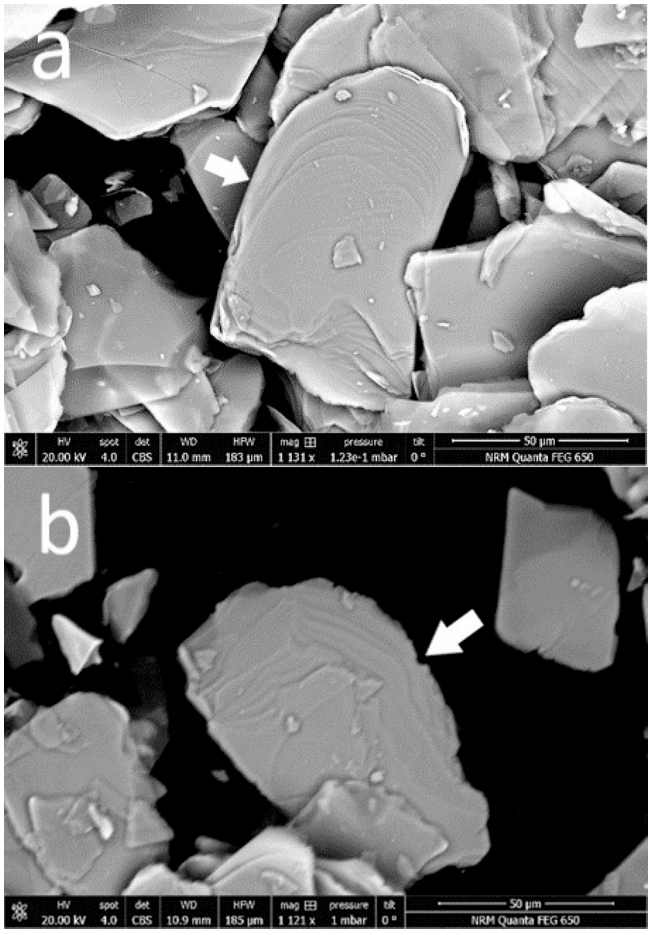

Fig. 2. FE-SEM images of biotite grains: a) before leaching, b) after leaching with KMW at pH 4. The bright parts in Fig 2a are due to local SEM charge-up effects, due to use of uncoated samples.

rates at pH 5 shows $1{\cdot}10^{-13}$ and $6{\cdot}10^{-13}$ mol m^{-2} s^{-1}, respectively (Nagy, 1995), which supports the assumption that muscovite dissolves at a slower rate than biotite. This corresponds to the evaluated final rates $R_\infty = 1{\cdot}10^{-13}$ (MSW series) and $3{\cdot}10^{-12}$ M s^{-1} (0 W series). Apparently, in the MSW series, muscovite also contributed to the Al concentration with a quicker dissolved Al fraction, presumably from fine particles.

4.7.2. Results of Fe_{tot} analyses

The Fe concentration data at pH 4 showed the expected initial rapid accumulation over time, which then levelled out. Like Al, the MSW series deviated from the other series, showing enhanced accumulation. All data series for pH 4 were successfully modelled by fitting Eq. (8) and are shown in Fig. 6.

At pH 6.5, all data showed lower accumulation compared to that at pH 4, as expected. However, for the FMW series, the concentration was lower than expected and seemed to be controlled by saturation with a secondary Fe mineral, most likely siderite $FeCO_3$ (s). The solubility of siderite in a 2 mM carbonate solution is expected to be approximately $3{\cdot}10^{-8}$ M ($pK_s = 10.2$, (Silva et al., 2002)), a value in good agreement with the initially measured values of total Fe for this series. Only the last measured value was in the range of the other series, which may indicate that siderite initially formed and finally dissolved. Alternatively, precipitation may have occurred specifically in the samples for ICP-MS because the corresponding samples for Fe(II) did not seem to be affected (see next section). It could have been the case that some samples were not acidified immediately or quickly enough to prevent the formation of a very small amount of non-soluble Fe precipitation. Because Fe_{tot} was probably restricted by precipitation in the FMW series at pH 6.5, the accumulation was not modelled. All other series (pH 6.5) were modelled by fitting Eq. (8) and are shown in Fig. 7.

The fitted model parameters for pH 4 and 6.5 are shown in Appendix D and Table D-2.

At pH 4, the fitted parameters were relatively similar for all series. However, just like results for Al, the MSW series with solid muscovite showed an enhanced initial rate, R_0. The presence of muscovite resulted in higher Al and Fe concentrations than in the other series; however, the final rate R_∞ was significantly lower than that of the other series, which was also the case for Al. Therefore, it can be assumed that muscovite contributes to an initial quickly released metal fraction but may then limit further accumulation of Al and Fe in the leaching solution.

At pH 6.5, the fitted rates were generally lower than those at pH 4, as expected, and the dissolution took a considerably longer time to approach the final dissolution rate. For the 0 W and KMW series, the fitted final rates at pH 6.5 were 2–3 orders of magnitude slower than those at pH 4. For the 0 W series, Fe accumulation was one order of magnitude faster than that for the KMW series, which may indicate that the additional components (K and/or Mg) in KMW have a certain inhibiting effect on Fe release from biotite. However, this was only the case for pH 6.5, as, at pH 4, the final dissolution rates were the same for the 0 W and KMW series. The data for the FMW series were not fitted because secondary mineral precipitation was suspected in the subsamples for ICP-MS analyses.

In addition, at pH 6.5, the muscovite-amended water series MEW and MSW had very low final rates of approximately 10^{-17} mol s^{-1}. The final concentrations were only slightly below the KMW series (approximately $2\ 10^{-5}$ M); thus, the presence of any limiting secondary phase was unlikely.

4.7.3. Results of Fe(II) analyses

Apart from the first sampling point, which was not measured in some cases, the Fe(II) concentration data for pH 4 were, as expected, very similar to the total Fe data reported in the previous section, with a notable exception for the MSW series (with muscovite particles), where the total Fe was significantly larger than the Fe(II) concentration. In the previous section, it was assumed that the muscovite present in the MSW series may have contributed additional Fe. The results for Fe(II) suggest that the contribution from muscovite was mainly Fe(III), which was apparently not reduced to Fe(II) during the experiments. Therefore, for the MSW series, only the Fe(II) dataset may have indicated "pure" biotite dissolution. All data series for Fe(II) at pH 4 were successfully modelled by fitting Eq. (8) and are shown in Fig. 6.

The Fe(II) data for pH 6.5 were relatively complicated to interpret. At pH 6.5, there was good agreement between the total Fe and Fe(II) data for the 0 W and KMW series. In addition, the FMW series Fe(II) data seemed to show the expected dissolution behaviour of biotite (the dissolution model could be fitted to the data), whereas the total Fe data showed typical signs of precipitation. In the previous section, this was specifically attributed to possible siderite precipitation in the subset of samples for ICP-MS that were not acidified quickly enough. Therefore, the Fe(II) data for the FMW series could be considered to indicate biotite dissolution in contrast to the total Fe data.

The main problem with the Fe(II) data at pH 6.5 was the muscovite-amended water series MEW and MSW, which both showed deviating values for Fe(II) compared with total Fe. However, this time, Fe(II) values were larger ($\sim 5{\cdot}10^{-5}$ M) than total Fe ($\sim 2{\cdot}10^{-5}$ M), suggesting that precipitation of Fe also occurred in the ICP-MS samples because of insufficient acidification of those samples. However, the total Fe values of approximately $2{\cdot}10^{-5}$ M were not low enough for any precipitation of siderite, which should typically be approximately $3{\cdot}10^{-8}$ M.

The relatively large Fe(II) concentrations of approximately $5{\cdot}10^{-5}$ M in the MEW and MSW series, an excess of $3{\cdot}10^{-5}$ M over the corresponding total Fe concentrations, can, therefore, only be explained by the presence of an element that specifically interferes with spectroscopic

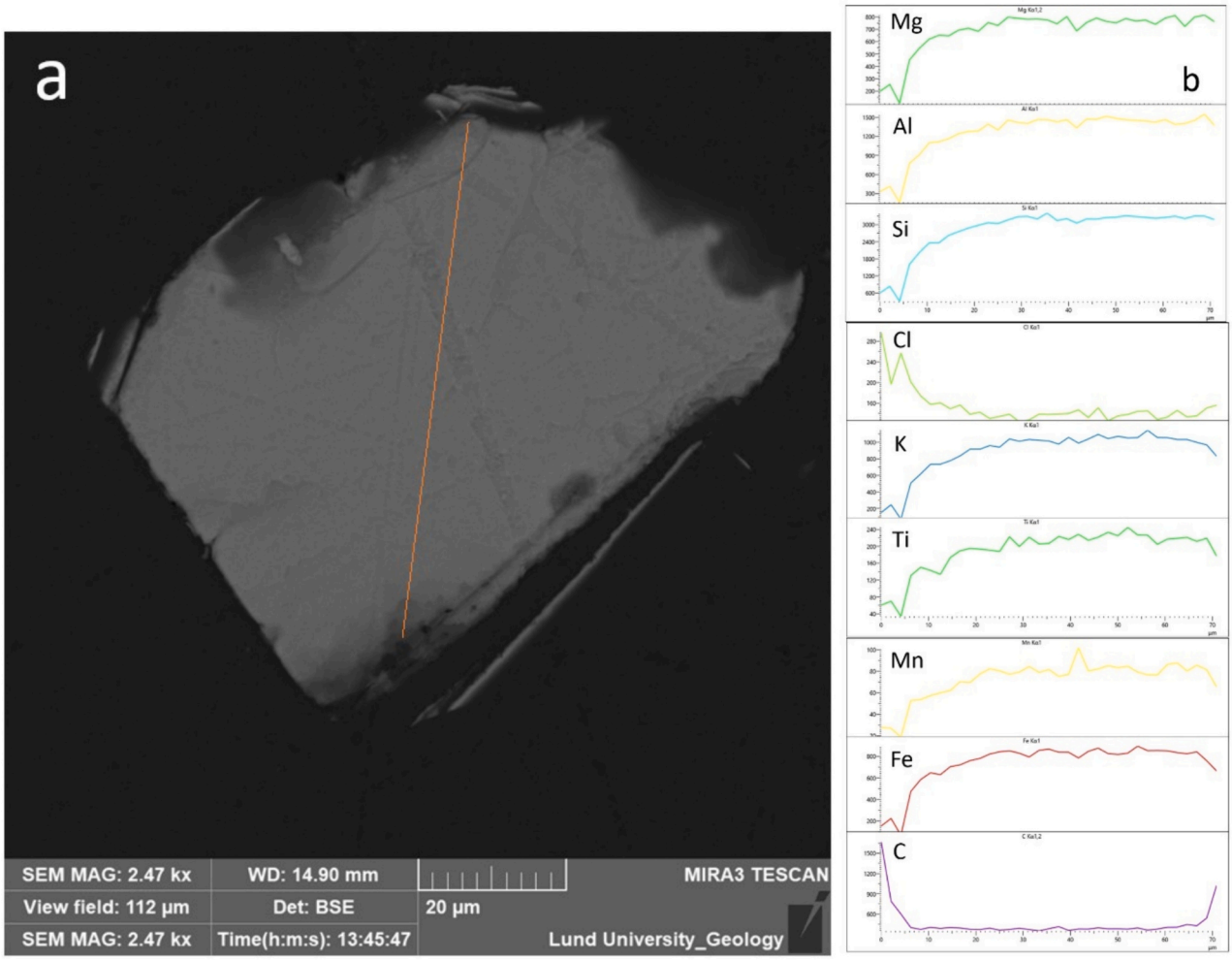

Fig. 3. a) FE-SEM image of a polished biotite grain section (sample #5, leaching conditions KMW pH 6.5). Line indicates the elemental mapping line-scan (from bottom to top), b) elemental line-scan mapping, left to right = from bottom to top in a).

Fe(II) analyses. Reported possible interferences with the Fe(II) analytical method are Cr, Zn, Co, and Cu (Lipps, 2022). From chemical analyses (Table 2) none of these metals were expected to be present in larger amount from muscovite compared with biotite. Ba and Sr originating from the muscovite may interfere, also the Mn present in biotite may interfere with Fe(II). To confirm whether this was the case or not, solutions of Mn, Ba and Sr in ppm range were prepared but these gave only normal Fe(II) blank values.

All the data series for Fe(II) at pH 6.5 were successfully modelled by fitting Eq. (8) and are shown in Fig. 7. However, the fitted parameters for the MEW and MSW series were likely influenced by suspected interference with the Fe(II) analyses.

The fitted model parameters for Fe(II) at pH 4 and 6.5 are shown in Appendix D and Table D-3.

For Fe(II) at pH 4, the fitted parameters were similar for all series and were like the total Fe content (Appendix D, Table D-2). The MSW series (containing solid muscovite) showed deviating results for total Fe but not for Fe(II). Therefore, it may be assumed that muscovite mainly contributed to the additional Fe(III) in the total Fe, whereas biotite mainly contributed to Fe(II).

At pH 6.5, the data for Fe(II) were very similar to those for the total Fe for the 0 W and KMW series. The Fe(II) data for the FMW series appeared not to be affected by precipitation, which was probably the case for total Fe. This problem is attributed specifically to the samples taken for ICP-MS analyses, which were probably left for too long before the subsamples were taken and acidified for the analyses.

Finally, the rates for the two series of MEW and MSW probably do not show pure Fe(II) accumulation but may show the presence of an interfering element (not identified) in muscovite-contacted water. The fast initial rate, followed by an extremely low final rate of approximately 10^{-19} mol s^{-1}, suggests a constant concentration of the interfering element in the MEW and MSW series. This interference should also be present in the corresponding series at pH 4. However, at this lower pH, the increased accumulation of Fe(II) probably overrides the interference element concentration, thereby masking its contribution to the signal.

The Fe(II) blanks that were prepared at pH 2.5 as indicators of Fe(II) stability are shown in Appendix B, Table B-3. Apart from the FMW series at pH 6.5, the values were close to the expected 2 ppm ($4{\cdot}10^{-5}$ M) Fe(II), more importantly the values were stable over time. This indicates that no air ingress has taken place during the experimental period. However, since both Fe(II) levels and pH are different from the main series of experiments, the results for these blanks cannot be used for estimating the actual O_2 levels in the biotite leaching experiments.

4.7.4. Results of Mn analyses

The Mn concentration data at pH 4 showed the expected initial rapid accumulation with time and then levelled out. Notably, the accumulated Mn concentrations were generally approximately one order of magnitude lower than those of Fe, reflecting the lower content of Mn than that of Fe in the biotite (Table 2). All series for Mn at pH 4 were successfully modelled by fitting Eq. (8), and all the data for pH 4 are shown in Fig. 8.

At pH 6.5, all the Mn data showed lower accumulation than at pH 4,

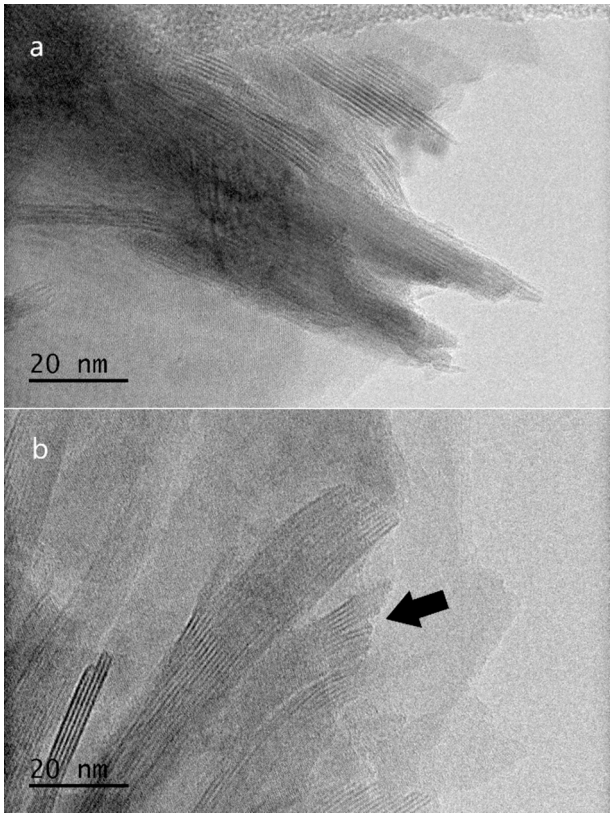

Fig. 4. TEM images of biotite a) pristine and b) leached samples. Arrow points to a flaring of sheet layers, possibly an effect of leaching.

as expected. Notably, Mn accumulation was much less affected by the pH change than Fe and was more like the Si data (below) in this respect. All the series for Mn at pH 6.5 were modelled by fitting Eq. (8), and all the data for pH 6.5 are shown in Fig. 9.

The fitted model parameters for Mn at pH 4 and 6.5 are shown in Appendix D and Table D-4.

The fitted rate parameters for Mn accumulation generally showed the expected lowest rates among all the elements investigated, apparently because of its relatively low content (0.7%) of this element in biotite compared with main elements Fe, Al, and Si (see Table 2). As expected, the rates at pH 6.5 were lower than those at pH 4, but the difference in rates between the two pH values was, unlike the results for Fe, very small.

This moderate difference in the rates between the two pH values was also observed for Si, indicating that Mn may not be primarily released from the octahedral layer but instead from the tetrahedral layer. The inclusion of divalent cations such as Mn(II) in the tetrahedral layer is, however, not very likely, but inclusion is possible for trivalent Fe(III) and them maybe also Mn(III).

4.7.5. Results of Si analyses

The Si concentration data at pH 4 showed the expected initial rapid accumulation over time, which then levelled out. Compared with Al the Si concentrations were generally higher by a factor of two, which can be expected from the biotite stoichiometry. As was the case for Al and Fe, the MSW series showed a significantly higher accumulation of Si than the other series, indicating a possible contribution from muscovite dissolution. All series for Si at pH 4 were successfully modelled by fitting Eq. (8), and all the data for pH 4 are shown in Fig. 10.

At pH 6.5, the Si accumulation was lower than that at pH 4, as expected, but the difference was not large, typically double or triple the amount and not by several orders of magnitude, which was observed for the octahedral layer element Fe. One notable exception was the muscovite-amended water (MEW) series, which, at pH 6.5, accumulated more Si than the corresponding series at pH 4; this exception from the general trend cannot be explained other than it must be a Si contamination issue. The error bars for the triplicates are also unusually large; therefore, this might be the result of spurious contamination with Si in one of the triplicate experiments of the MEW series at pH 6.5. All the series for Si at pH 6.5 were modelled by fitting Eq. (8), and all the data for pH 6.5 are shown in Fig. 11.

The fitted model parameters for Si at pH 4 and 6.5 are shown in Appendix D and Table D-5.

The fitted rate parameters for Si accumulation generally show comparatively minor differences between the two pH values, indicating that Si dissolution is only weakly dependent on pH in this pH interval. The total dissolved Si may also be used as a proxy for amount of biotite dissolved. A calculation for 0 W conditions at pH 4 and 6.5 gives $1.5{\cdot}10^{-6}$ and $4.6{\cdot}10^{-7}$ mol dissolved Si, respectively. This corresponds

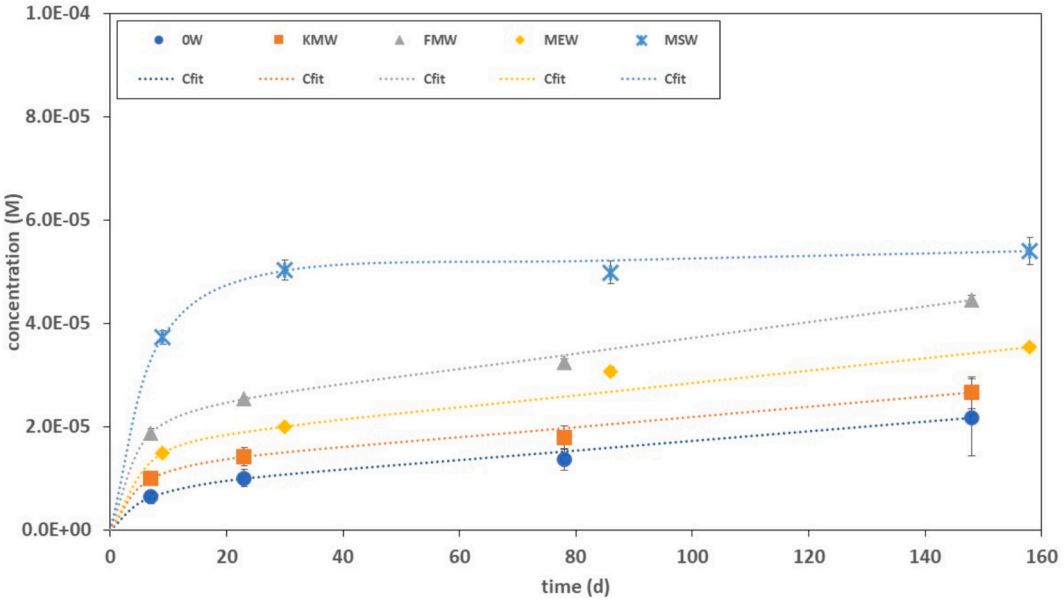

Fig. 5. The accumulation of Al in biotite leaching solutions at pH 4 for the five different water types. Lines are the fitted model. Water codes: see Table 3.

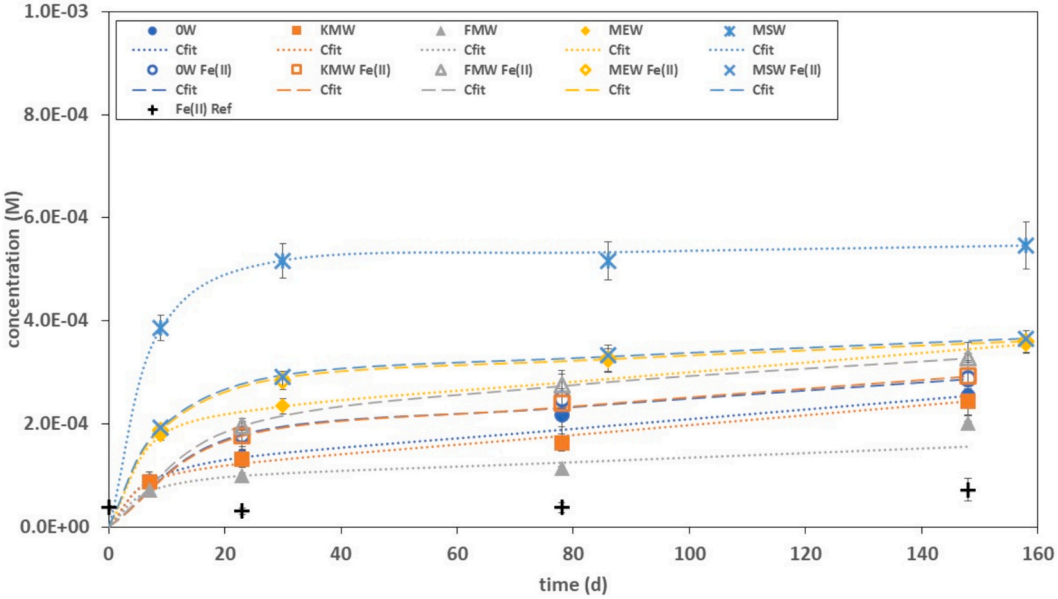

Fig. 6. The accumulation of total Fe (filled symbols and stars) and Fe(II) (open symbols and x-crosses) in biotite leaching solutions at pH 4 for the five different water types. Crosses = Fe(II) blanks. Lines are the fitted model. Water codes: see Table 3.

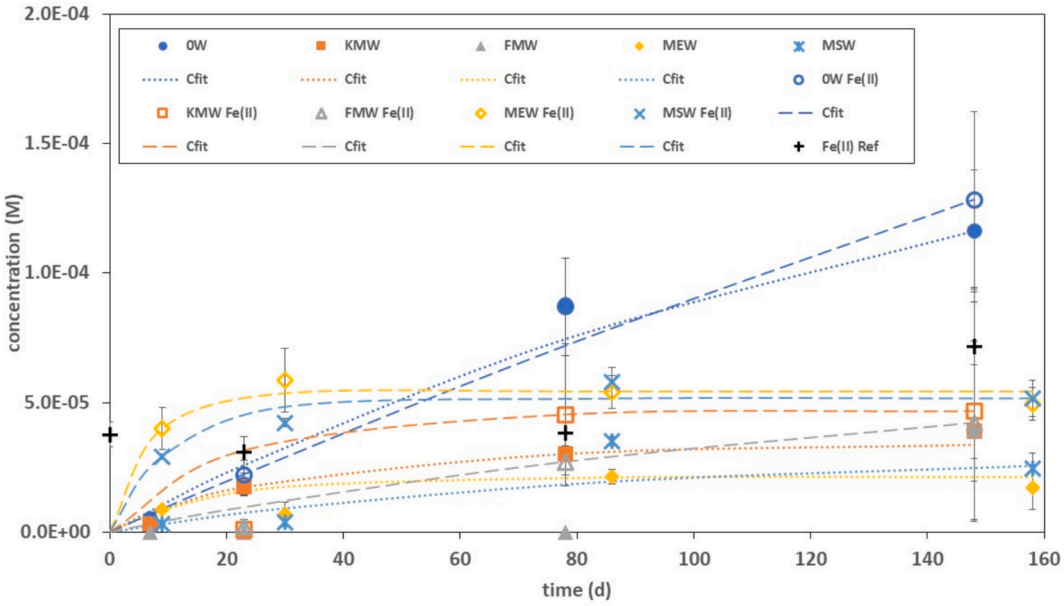

Fig. 7. The accumulation of total Fe (filled symbols and stars) and Fe(II) (open symbols and x-crosses) in biotite leaching solutions at pH 6.5 for the five different water types. Crosses = Fe(II) blanks. Lines are the fitted model. Water codes: see Table 3.

to 0.56 and 0.17% dissolved biotite, respectively.

4.8. Normalisation of dissolution rates

For comparison of the dissolution rates attained for the different elements under different leaching conditions, presented in Appendix D, these rates must first be normalised with the measured stoichiometric factors for the respective indicator element; second, if a comparison is to be made with literature values, all the rates must additionally be normalised with both SSA and the leaching solution volume.

Normalisation was performed using the stoichiometric factors measured from the chemical analyses. The post-leaching SSA value of 0.87 m^2/g was used (Table 5) for normalisation of the final rates R_∞, as this is supposedly a measurement of pure main fraction, where most of the fine particles are removed. The fine particle dissolution rates R_0 were not normalised or used for comparison only because the amount of fines present was unknown (the relative amount is probably very small).

The amount of biotite was 0.05 g, and the solution volume was 0.02 L in each experiment. This presents a correction factor of 0.02/0.87/0.05 = 0.46 L m^{-2} that is applied to all the final rates presented in Appendix D. The normalised rates are presented in Table 7 below.

The italicised values in Table 7 are very similar at pH 4 and are significantly larger than the boldfaced values at this pH, whereas at pH 6.5, they are significantly lower than the boldfaced values. Because the values are related to Fe, Fe(II), and Mn (at pH 4), it can be assumed that these values are related to the dissolution of the octahedral layer. This layer is particularly susceptible to proton attack, probably owing to the exchange of the cation interlayer potassium, thereby creating a charge

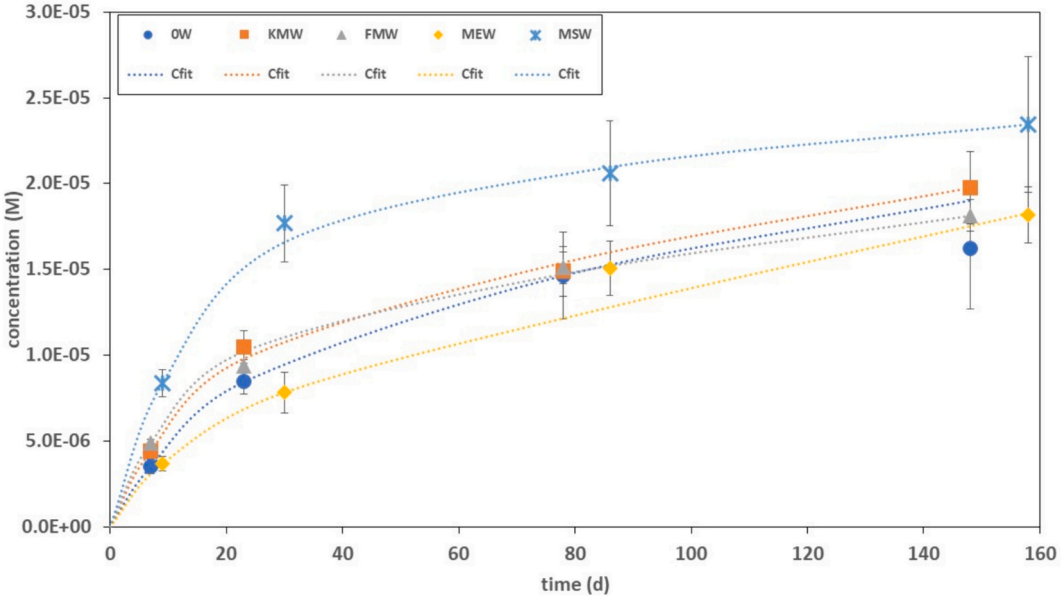

Fig. 8. The accumulation of Mn in biotite leaching solutions at pH 4 for the five different water types. Lines are the fitted model. Water codes: see Table 3.

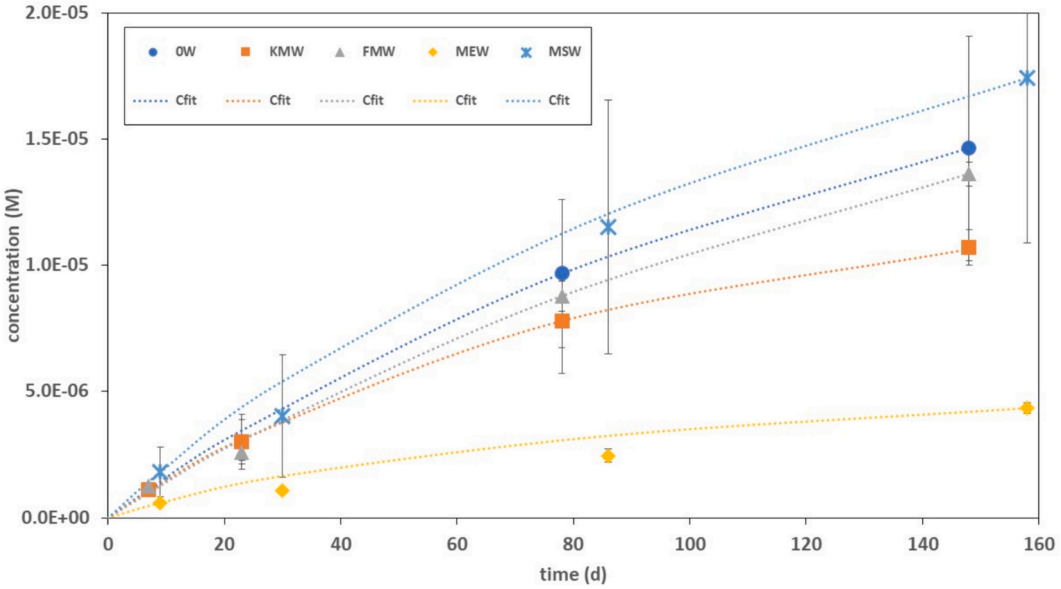

Fig. 9. The accumulation of Mn in biotite leaching solutions at pH 6.5 for the five different water types. Lines are the fitted model. Water codes: see Table 3.

imbalance. In contrast, at pH 6.5, the layer is still protected by the interlayer K.

Because the boldfaced group of values in Table 7 concerns mainly Si and Al (and Mn at pH 6.5), these are probably related to the dissolution of the tetrahedral layer, which is only weakly connected to pH and is apparently much less susceptible to proton attack. The rates were only marginally enhanced at pH 4 compared to the values at pH 6.5. This concerns Si, Al, and possibly Mn to some extent. The latter element shows relatively ambiguous behaviour: it follows Fe at a lower pH but Si at a higher pH value. This may be because Mn is not a major constituent of biotite, and because of its low concentration, the data may be more uncertain.

The normalised rates, presented in Table 7, for Fe, Fe(II), Mn, and Si were evaluated separately for the proton-independent dissolution rate coefficient, k_{H+} and the proton reaction order number, n_{H+}, according to Eq. (4). Al was not evaluated because pH 6.5 data were missing. The results are also shown in Table 8 and Fig. 12.

In Fig. 12, a prominent difference exists in the behaviour between the octahedral sheet element Fe and the tetrahedral sheet element Si, which shows the nature of the incongruent dissolution of biotite. The Fe dissolution rates show a much stronger dependency on the proton concentration than the Si dissolution rate. This is indicated by the difference in n_{H+} for Fe and Si, as well as by the difference in the linear regression correlation coefficients (Table 8). The values of n_{H+} for Fe and Fe(II) are comparable with those previously reported in the literature (about 0.5–0.9, see Table 1), however, as already have been remarked, the spread in the literature values for this parameter is also quite large. The value of $n_{H+} = 0.09$ for Si is, on the other hand, remarkably low when compared with literature data (about 0.2–0.9, see Table 1).

The results revealed that biotite dissolution was incongruent, as well as that the degree and "sign" of incongruent dissolution were also

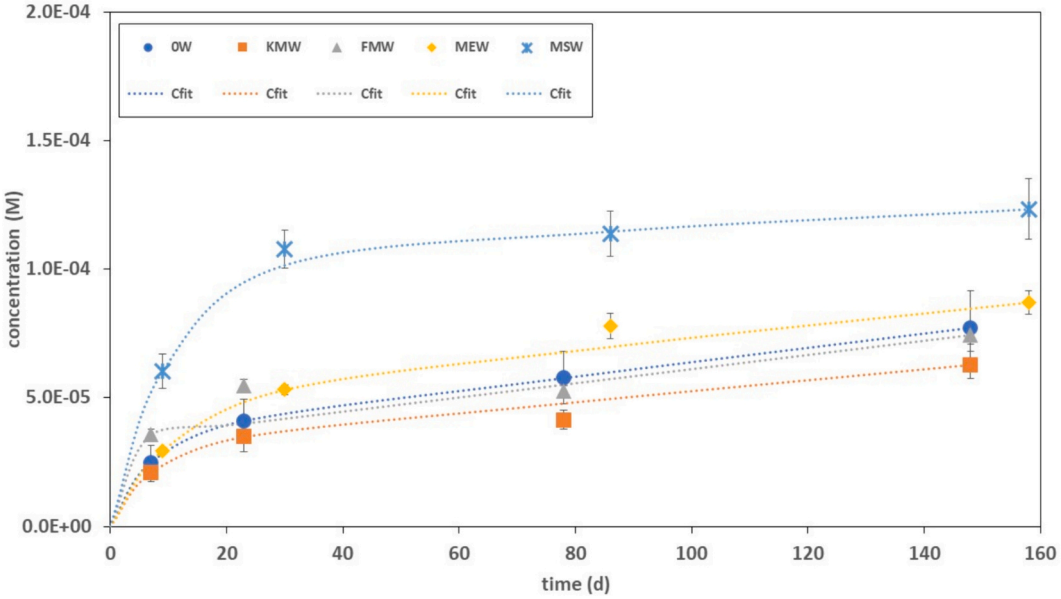

Fig. 10. The accumulation of Si in biotite leaching solutions at pH 4 for the five different water types. Lines are the fitted model. Water codes: see Table 3.

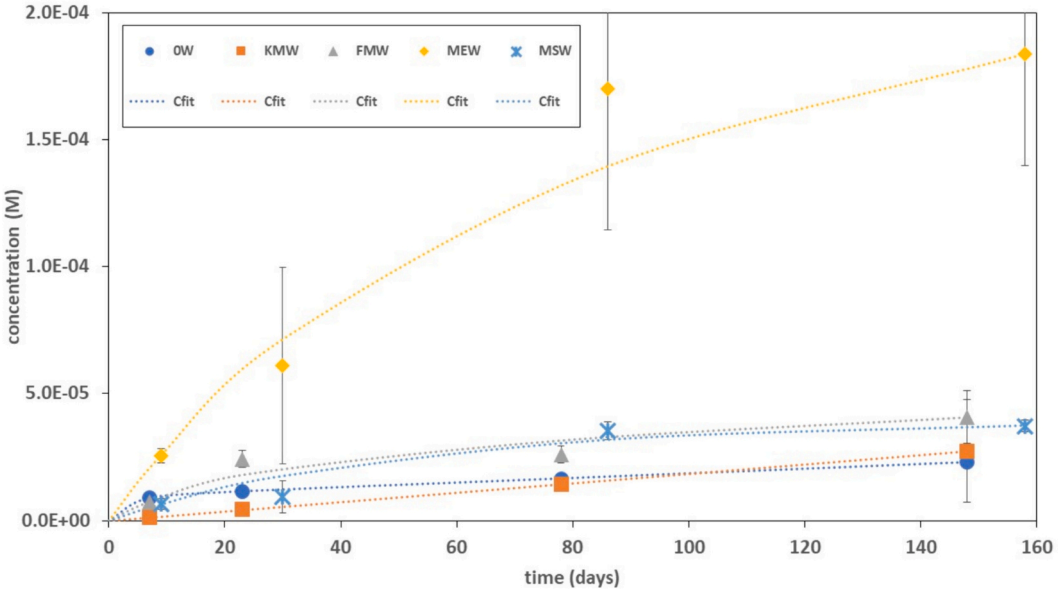

Fig. 11. The accumulation of Si in biotite leaching solutions at pH 6.5 for the five different water types. Lines are the fitted model. Water codes: see Table 3.

Table 7
Comparison of normalised dissolution rates (mol s^{-1} m^{-2}) for the five different biotite dissolution indicators. S.f = stoichiometric factor. Bracketed values are probably affected by contaminations. In Table 7, the similarity in values is indicated by one group with values written in italics and the other group written in boldface.

	Final pH	Al (s.f. = 1.3)	Fe (s.f. = 2.1)	Fe(II) (s.f. = 1.9)	Mn (s.f. = 0.1)	Si (s.f. = 2.6)
0 W-4	4.17	**$3.8{\cdot}10^{-13}$**	*$2.4{\cdot}10^{-12}$*	*$2.2{\cdot}10^{-12}$*	*$3.2{\cdot}10^{-12}$*	**$5.7{\cdot}10^{-13}$**
KMW-4	4.20	**$4.0{\cdot}10^{-13}$**	*$2.4{\cdot}10^{-12}$*	*$2.4{\cdot}10^{-12}$*	*$3.3{\cdot}10^{-12}$*	**$4.4{\cdot}10^{-13}$**
FMW-4	4.16	**$6.3{\cdot}10^{-13}$**	*$1.1{\cdot}10^{-12}$*	*$2.1{\cdot}10^{-12}$*	*$2.6{\cdot}10^{-12}$*	**$5.6{\cdot}10^{-13}$**
MEW-4	4.09	**$4.9{\cdot}10^{-13}$**	*$2.4{\cdot}10^{-12}$*	*$1.4{\cdot}10^{-12}$*	*$2.0{\cdot}10^{-10}$*	**$4.9{\cdot}10^{-13}$**
MSW-4	4.08	**$1.0{\cdot}10^{-13}$**	*$4.6{\cdot}10^{-13}$*	*$1.4{\cdot}10^{-12}$*	*$4.0{\cdot}10^{-12}$*	**$2.5{\cdot}10^{-13}$**
0 W-6	6.64	n.a.*	*$3.6{\cdot}10^{-14}$*	*$1.5{\cdot}10^{-14}$*	**$2.7{\cdot}10^{-13}$**	**$1.9{\cdot}10^{-13}$**
KMW-6	6.51	n.a.*	*$6.3{\cdot}10^{-14}$*	*$1.9{\cdot}10^{-14}$*	**$7.1{\cdot}10^{-14}$**	**$3.8{\cdot}10^{-13}$**
FMW-6	6.96	n.a.*	n.a.*	*$1.9{\cdot}10^{-13}$*	**$4.8{\cdot}10^{-13}$**	**$2.5{\cdot}10^{-13}$**
MEW-6	6.57	n.a.*	$1.4{\cdot}10^{-17}$	($1.4{\cdot}10^{-18}$)	**$5.8{\cdot}10^{-13}$**	**$8.3{\cdot}10^{-13}$**
MSW-6	6.54	n.a.*	$1.4{\cdot}10^{-17}$	($1.4{\cdot}10^{-18}$)	$2.5{\cdot}10^{-12}$	$2.7{\cdot}10^{-14}$

* Not analysed due to suspected precipitation.

Table 8
Evaluated pH-independent rate coefficients k_{H+} and proton reaction orders n_H.

	Fe	Fe(II)	Mn	Si
k_{H+} (mol^{1-n} s^{-1} m^{-2})	$4.8 \bullet 10^{-10}$	$6.9 \bullet 10^{-10}$	$6.3 \bullet 10^{-11}$	$1.0 \bullet 10^{-12}$
n_{H+}	0.61	0.63	0.33	0.09
Regression coefficient	0.87	0.80	0.55	0.41

dependent on the pH value. At pH 6.5, the incongruent dissolution was "reversed" from pH 4; the tetrahedral layer element Si dissolved faster than the octahedral element Fe and at one point, at approximately pH 5, the dissolution can be supposed to be congruent according to Fig. 12. This change in the preferential release of octahedral elements at low pH and tetrahedral elements at neutral pH was also shown in a previous study (Malmström and Banwart, 1997). The point of congruent dissolution, at approximately pH 5, probably coincide with a pK_a value of the biotite edge surface groups (Malmström and Banwart, 1997). Therefore, it can be assumed that the edge sites of biotite can soak up protons until approximately this pK_a value is reached; at lower pH, the potassium of the exchange sites near the edges then starts to exchange with protons, and consequently, the dissolution of the octahedral layers accelerates.

The release of Fe_{tot} is probably a mixture of Fe(II) and Fe(III) released from the octahedral layer and possibly some additional Fe(III) released from the tetrahedral layer. Therefore, one may expect corresponding differences in the Fe(II) and Fe_{tot} rates. The Fe_{tot} rates should be enhanced over Fe(II) rates at pH 6.5 and vice versa at pH 4, and this is also evident in Fig. 12, where the pH-dependent rates of the purely octahedral indicator Fe(II) show the steepest slope, although not substantially ($n_H = 0.63$ for Fe(II) compared with $n_H = 0.61$ for Fe_{tot}).

This finding is also supported by the Mössbauer spectroscopic results for the Fe(III)/Fe_{tot} ratio. The Results (Section 4.3) showed that biotite leached at pH 4 had a ratio of 13.0%, whereas the biotite leached at pH 6.5 had a ratio of 11.6%. These figures were compared with the pristine sample, which had a ratio in between of these at 12.1%. Because the octahedral layers mainly contain Fe(II) and the tetrahedral layers contain Fe(III), one may interpret these results as the Fe(III)/Fe_{tot} ratio increasing at pH 4 due to preferential octahedral leaching but decreasing at pH 6.5, owing to preferential tetrahedral leaching. The differences in the measured ratios were small; but they do not contradict the results from the analyses of the leaching solutions.

The different leaching conditions investigated seemed to have negligible effect on the leaching rates of biotite at pH 4 (Table 7); with a few exceptions, all rates were similar for a given element and pH value. At pH 6.5, the muscovite-amended contact solutions had significantly higher initial rates but lower final rates of Fe dissolution. The presence of muscovite likely complicates the release pattern of Fe from biotite dissolution. However, neither the Mn nor Si release rates appear to be affected by muscovite; therefore, the actual dissolution of biotite may not be affected by the presence of muscovite.

The build-up or presence of secondary phases, such as vermiculite, could not be established neither by XRD nor by TEM, probably because such phases are, at least initially, highly amorphous. The FE-SEM elemental line-scan investigations suggested that some elemental depletion occurred near the edges of the biotite grains. According to one study, dissolved Si builds up at the biotite grain edges and ultimately saturates the solution with respect to SiO_2(am) (Turpault and Trotignon, 1994). However, no accumulation of Si near the biotite grain edges was observed in the FE-SEM elemental line scans made in this study (Fig. 3).

4.9. Comparison with previous studies

To compare the results obtained here, under anaerobic conditions, with the literature data presented in Table 1, a certain pH value was selected, and the rates at this specific pH value were then calculated for comparison. pH 5 was selected for comparison, partly because the empirical model by (White and Brantley, 2003) was fitted to the collected literature data from approximately this pH (actual range pH 3–7) and partly because it is at this approximate pH value that congruent dissolution can be assumed to occur, at least according to the findings in the previous section.

Therefore, using the collected literature data for the pH-independent coefficients and reaction order values from Table 1, biotite dissolution rates at pH 5 were calculated and are shown in Fig. 13, together with the model for biotite dissolution by (White and Brantley, 2003) Eq. (5) (solid line).

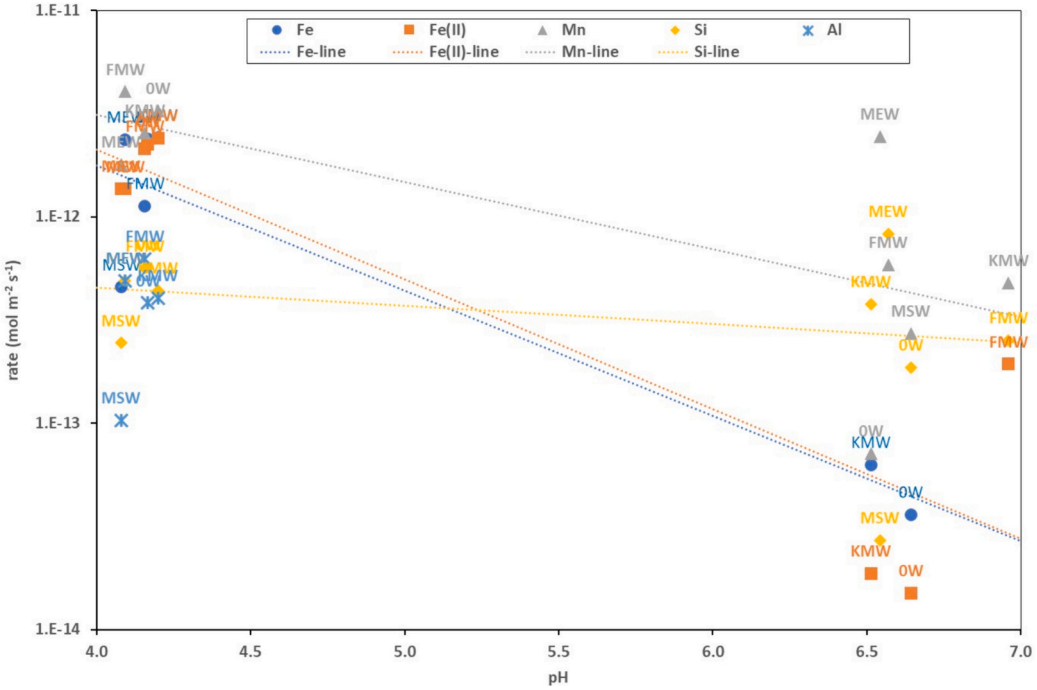

Fig. 12. Normalised dissolution rates versus pH value. Labels indicate the type of leaching water (Table 3).

In addition, Fig. 13 shows the model proposed in this study (Eq. (7)), which was fitted to the literature data (using the stated time length of the respective experiments), together with the data obtained here for Fe, Si, and Mn (Table 8), adjusted to pH 5. This fit yielded a final dissolution rate R_∞ of $10^{-12.46}$ mol m^{-2} s^{-1}.

This value for laboratory biotite dissolution rate at pH 5 can also be compared with an estimated field biotite dissolution rate of $10^{-12.92}$ mol m^{-2} s^{-1} at pH 5–6 (Velbel, 1985) and a recommended general value for the dissolution rates of sheet silicates of $10^{-13\pm0.5}$ mol m^{-2} s^{-1} at pH 5 and 25 °C (Nagy, 1995). In the latter review, the value from laboratory experiments, specifically for biotite dissolution at pH 5, is $10^{-12.2}$ mol m^{-2} s^{-1}, a value cited from (Acker and Bricker, 1992). In a recent review and by fitting T dependent far from equilibrium data to Eq. (1), best fit values for biotite gave the values $k_{H+} = 3.8{\cdot}10^{-10}$ ($mol^{0.5}$ m^{-2} s^{-1}) and and $n_{H+} = 0.5$ (Hermanska et al., 2022). At pH 5 this gives a rate value of $10^{-11.9}$ mol m^{-2} s^{-1}.

According to Fig. 13, most literature data are very close to the line of the biotite dissolution rate model proposed here for describing the effect of the fine particles on laboratory data, Eq. (7), and also the line of the model proposed by (White and Brantley, 2003), that is Eq. (5), which is also based on long-term weathering studies. Thus, it seems possible to integrate most laboratory data for biotite dissolution, whether they are made at aerobic or anaerobic conditions, even if there are large differences in the amount of secondary mineral formation and the BET areas of biotite found in these studies. One can also note that the literature data in Table 1 and Fig. 13 is based on both batch and flow-through type of reactors. Provided that batch reactors are used as semi-open systems with regular water changes, both type of reactors should then operate at far-from equilibrium conditions and rate data should be comparable, which also seems to be the case.

4.10. Consequences for biotite weathering

According to the results of this study, the observable effect of anaerobic conditions on dissolution rate of biotite seems to be comparatively small. For longer time scales and stagnant water zones, the gradual build-up of secondary minerals may start to influence the surface reactivity by limited diffusion-controlled access, and the dissolution rate may decrease further, as the parabolic model by (White and Brantley, 2003) suggests. The lack of evidence for vermiculite formation in this study may indicate that such secondary mineral formation may be slower at anaerobic than aerobic conditions where the formation of secondary products are reported in post-leaching spectroscopic examinations. In a previous anaerobic dissolution study of biotite, probably with more reactive conditions (pH 4.6 at 100 °C), vermiculite did form but then incorporated Fe(II) instead of Fe(III) found at aerobic conditions. It suggests that further transformations of secondary minerals may lead to different end products (Murakami et al., 2004).

4.11. Estimation of the remediation time for reducing conditions

To estimate the time required for remediation of the reducing conditions in the rock at the waste repository depth after cutting off contact with the atmosphere, a simple calculation of the equilibrium conditions can be made. This calculation disregards any transport of groundwater and dissolved matter that may occur within the porous system of the rock.

If one considers a cubic slab of rock with a size of 1 m^3 and with a measured porosity of 0.23% (Selnert et al., 2008), this contains a volume of 2.3 L of groundwater. A PHREEQC (Parkhurst and Appelo, 2021) calculation with the LLNL database of thermodynamic constants for the water of the Forsmark type (KFM02A 509–516 m) (Byegård et al., 2006) and at a temperature of 10 °C, results in a dissolved O_2 concentration of $2.5{\cdot}10^{-4}$ mol/kg (8 ppm), that is, approximately $5.75{\cdot}10^{-4}$ mol of dissolved oxygen in the porewater of 1 m^3 of rock.

Then, using the measured 0.015 m^2/g BET-SSA value of the drill core samples from the same borehole (KFM02A) at Forsmark (André et al., 2009) and a density of 2700 kg/m^3 of this rock type (Selnert et al., 2008), this results in an available pore surface area of 4050 m^2.

The content of biotite in this rock type varies between 3 and 12% (Selnert et al., 2008), with an average value of 7.5%. Assuming that this is also the percentage of the biotite surface available, the area of biotite available for dissolution was estimated to be approximately 300 m^2.

If one applies a Fe(II) dissolution rate of $6.9{\cdot}10^{-10} \cdot \{10^{-7}]^{0.63} =$

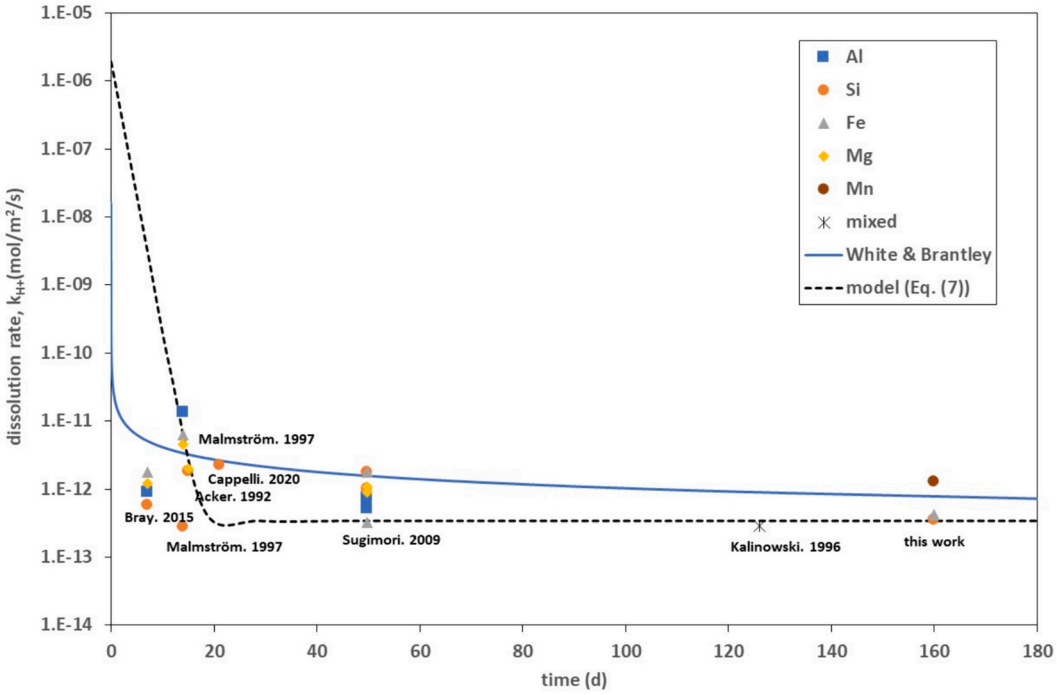

Fig. 13. Comparison of literature data with results of this work for the dissolution of biotite at pH 5 as a function of duration of experiments, showing four different indicator elements and one point with mixed elemental data. Lines are models (see text).

$2.7{\cdot}10^{-14}$ mol m^{-2} s^{-1} at a neutral pH value of 7 from the parameters evaluated from experimental data in Table 8, and neglecting any contribution of Fe from hydroxide leaching of biotite and considers a reaction.

$$4\ Fe^{2+} + O_2(aq) + 4H^{+} \Rightarrow 4\ Fe^{3+} + 2\ H_2O$$

This provides an oxygen consumption rate that is one-fourth of the Fe (II) dissolution rate or $6.71{\cdot}10^{-15}$ mol m^{-2} s^{-1}, or $2.01{\cdot}10^{-12}$ mol s^{-1} for the available biotite surface area. The estimated time it takes to consume $5.75{\cdot}10^{-4}$ mol oxygen is then 9 years after water saturation. Similar estimations have also been made by (Malmström et al., 1996), who estimated the time to be 52 years based on the iron release rate, and (Taylor and Owen, 1997), who estimated the time to be 50 years.

The estimation of the remediation time does not consider any build-up of secondary minerals because they have not been found in the leaching experiments on which the estimation is based. However, as shown in the previous section, the leaching rates obtained here were fully consistent with most literature data, where secondary minerals, typically vermiculite and/or hydrobiotite, have been proven to form.

5. Conclusions

In this study, anaerobic dissolution of biotite was investigated. The dissolution data were successfully interpreted using a dissolution rate model formulated based on the assumption of the presence of two types of solid fractions: the main fraction and fine particles.

Anaerobic conditions were maintained throughout the experiments by measuring total Fe and Fe(II), which showed very good agreement for almost all conditions. The separate Fe(II) blanks also exhibited stable concentrations.

For some experimental conditions, more specifically in the presence of muscovite or a muscovite-amended leaching solution, a discrepancy existed between the measured Fe_{tot} and Fe(II), most probably due to the presence of an unidentified element originating from muscovite, which interfered with the Fe(II) analyses.

By evaluating the behaviour of Al, Fe, Fe(II), Mn, and Si, the dissolution of biotite was proven to be incongruent, with octahedral Fe and tetrahedral Al and Si dissolving at different rates. This finding is consistent with that of several other studies conducted under aerobic conditions (Acker and Bricker, 1992) (Kalinowski and Schweda, 1996) (Malmström and Banwart, 1997).

The nature of this incongruent dissolution was highly dependent on the pH value. Octahedral sheets preferentially dissolved over tetrahedral sheets at low pH values. At higher pH values, the octahedral sheet became more stable, and at pH 6.5, the situation was reversed; the tetrahedral sheet dissolved faster than the octahedral sheet. At a pH approximately equal to the first surface pK_a of biotite ($pK_a \sim 5$ for edge surfaces according to (Malmström and Banwart, 1997), the dissolution of biotite can be supposed to be congruent.

This pH-dependent behaviour of biotite dissolution was supported, even if not confirmed, by the minor differences, when comparing the Fe (III)/Fe_{tot} ratios for pristine and leached biotite.

XRD, TEM and FE-SEM investigations showed that the degree of primary mineral alterations after leaching was small. The edges of the grains showed only a slight depletion of the main constituents owing to dissolution. The removal of fine particles combined with very little mineral alteration of the main size fraction also corresponded well with the analysed decrease in the specific surface area of leached biotite.

By the comparison of dissolution rate data from previous biotite dissolution studies, adjusted to pH 5, and for both aerobic and anaerobic conditions, this study proves that most of the discrepancies that exist between previously published laboratory data can be explained by the assumption of the presence of fine particles that will provide enhanced leaching rates for experiments that have been conducted during a relatively short period of time.

The anaerobic conditions used in this study did not indicate any significantly different biotite dissolution rates when compared with literature data, which were mainly obtained under aerobic conditions. Therefore, it can be concluded that biotite dissolution will occur at the same rate regardless of whether oxygen is present or not, at least in laboratory studies of fresh biotite material. This is an important observation, not least for the safety assessment of spent nuclear fuel waste repositories.

CRediT authorship contribution statement

Stellan Holgersson: Writing – review & editing, Writing – original draft, Resources, Methodology, Investigation, Formal analysis, Data curation, Conceptualization. **Henrik Drake:** Writing – original draft, Methodology, Investigation, Formal analysis, Data curation. **Andreas Karlsson:** Writing – original draft, Methodology, Investigation, Formal analysis, Data curation. **Lindsay Krall:** Writing – review & editing, Resources, Project administration, Methodology, Funding acquisition, Conceptualization.

Declaration of competing interest

The authors declare the following financial interests/personal relationships which may be considered as potential competing interests:

Stellan Holgersson reports financial support and writing assistance were provided by Swedish Nuclear Fuel and Waste Management Co. Lindsay Krall reports a relationship with Swedish Nuclear Fuel and Waste Management Co If there are other authors, they declare that they have no known competing financial interests or personal relationships that could have appeared to influence the work reported in this paper.

Data availability

Data will be made available on request.

Acknowledgement

This work was financially supported by the Swedish Nuclear Fuel and Waste Management Company (SKB). Dr. Daniel Madsen, Lund University is acknowledged for assistance with TEM analyses. We thank Dr. Birgitta Kalinowski for her valuable comments regarding this manuscript.

Appendix A. Supplementary data

Supplementary data to this article can be found online at https://doi.org/10.1016/j.chemgeo.2024.122204.

References

Aagaard, P., Helgeson, H.C., 1982. Thermodynamic and kinetic constraints on reaction rates among minerals and aqueous solutions. I. Theoretical considerations. Am. J. Sci. 282, 237–285.
Acker, J.G., Bricker, O.P., 1992. The influence of pH on biotite dissolution and alteration kinetics at low temperature. Geochim. Cosmochim. Acta 56, 3073–2092.
André, M., Malmström, M.E., Neretnieks, I., 2009. Specific surface area determination on intact drillcores and evaluation of extrapolation methods for rock matrix surfaces. J. Contam. Hydrol. 110, 1–8.
Bray, A.W., et al., 2015. Effect of pH, grain size, and organic ligands on biotite weathering rates. Geochim. Cosmochim. Acta 164, 127–145.
Brindley, G.W., Zalba, P.E., Bethke, C.M., 1983. Hydrobiotite, a regular 1:1 interstratification of biotite and vermiculite layers. Am. Mineral. 68, 420–425.
Brunauer, S., Emmet, P.H., Teller, E., 1938. Adsorption of gases in multimolecular layers. J. Am. Chem. Soc. 60, 309–319.
Byegård, J., Gustavsson, E., Tullborg, E.-L., Selroos, J.-O., 2006. Bedrock transport properties- Preliminary site description Forsmark area, version 1.2 (R-05-86). Svensk Kärnbränslehantering AB, Stockholm.
Cappelli, C., Cama, J., Van Driessche, E.S., Huertas, F.J., 2020. Biotite reactivity in nitric and oxalic acid at low temperature and acid pH from surface and bulk dissolution measurements. Chem. Geol. 554, 119806.

Coleman, N., Leroux, F., Cady, J., 1963. Biotite-hydrobiotite-vermiculite in soils. Nature 198, 409–410.
Crundwell, F.K., 2017. Path from reaction control to equilibrium constraint for dissolution reactions. ACS Omega 2, 4845–4858.
Drake, H., Sandström, B., Tullborg, E.-L., 2006. Mineralogy and geochemistry of rocks and fracture fillings from Forsmark and Oskarshamn: Compilation of data for SR-Can (R-06-109). Svensk Kärnbränslehantering AB, Stockholm.
Dubois, I., 2011. Specific surface area of some minerals commonly found in granite. Kungliga Tekniska Högskolan, Stockholm.
Dyar, M.D., Burns, R.G., 1986. Mössbauer spectral study of ferruginous one-layer trioctahedral micas. Am. Mineral. 71, 955–965.
Eyring, H., 1935. The Activated complex in chemical reactions. J. Chem. Phys. 3, 107–115.
Ferrow, E.A., Kalinowski, B.E., Veblen, D.R., Schweda, P., 1999. Alteration products of experimentally weathered biotite studied by high resolution TEM and Mössbauer spectroscopy. Eur. J. Mineral. 11, 999–1010.
Fordham, A.W., 1990. Weathering of biotite into dioctahedral clay minerals. Clay Miner. 25, 51–63.
Gautier, J.-M., Oelkers, E.H., Schott, J., 1994. Experimental study of K-feldspar dissolution rates as a function of chemical affinity at 150C and pH 9. Geochim. Cosmochim. Acta 58, 4549–4560.
Haward, S.J., et al., 2011. In situ atomic force microscopy measurements of biotite basal plane reactivity in the presence of oxalic acid. Geochim. Cosmochim. Acta 75, 6870–6881.
Hermanska, M., et al., 2022. A comprehensive and internally consistent mineral dissolution rate database: Part I: Primary silicate minerals and glasses. Chem. Geol. 597, 120807.
Kalinowski, B.E., Schweda, P., 1996. Kinetics of muscovite, phlogopite and biotite dissolution and alteration at pH 1–4, room temperature. Geochim. Cosmochim. Acta 60, 367–385.
Lasaga, A.C., 1995. Fundamental approaches in describing mineral dissolution and precipitation rates. Rev. Mineral. 31, 23–86.
Lipps Baxter., Braun-Howland (Ed.), 2022. Standard methods for the examination of water and waste water, 24th ed. American Water Works Association.
Malmström, M., Banwart, S., 1997. Biotite dissolution at 25C: The pH dependence of dissolution rate and stoichiometry. Geochim. Cosmochim. Acta 61, 2779–2799.
Malmström, M., et al., 1996. The dissolution of biotite and chlorite at 25C in the near-neutral pH region. J. Contam. Hydrol. 21, 201–213.
May, H.M., Helmke, P.A., Jackson, M.L., 1979. Gibbsite solubility and thermodynamic properties of hydroxy-aluminium ions in aqueous solutions. Geochim. Cosmochim. Acta 43, 861–868.
Murakami, T., et al., 2004. Anoxic dissolution processes of biotite: implications for Fe behaviour during Archean weathering. Earth Planet. Sc. Lett. 224, 117–129.
Nagy, K.L., 1995. Dissolution and precipitation kinetics of sheet silicates. Rev. Mineral. Geochem. 31, 173–233.
Nesse, W.D., 2000. Introduction to mineralogy. Oxford University Press, New York.
Oelkers, E.H., 2001. General kinetic decription of multioxide silicate mineral and glass dissolution. Geochim. Cosmochim. Acta 65, 3703–3719.
Oelkers, E.H., Schott, J., Devidal, J.-L., 1994. The effect of aluminium, pH, and chemical affinity on the rates of aluminosilicate dissolution rates. Geochim. Cosmochim. Acta 58, 2011–2024.
Parkhurst, D.L., Appelo, C.A.J., 2021. PHREEQC version 3: Computer Program for Speciation, Batch-Reaction, One-Dimensional Transport, and Inverse Geochemical Calculations. .. U.S. Geological Survey.
Prescher, C., McCammon, C., Dubrovinsky, L., 2012. MossA: a program for analyzing energy-domain Mössbauer spectra from conventional and synchrotron sources. J. Appl. Crystallogr. 45, 329–331.
Redhammer, G.J., et al., 2000. Spectroscopic and structural properties of synthetic micas on the annite-siderophyllite binary: Synthesis, crystal structure refinement, Mössbauer, and infrared spectroscopy. Am. Mineral. 85, 449–465.
Rieder, M., et al., 1998. Nomenclature of the micas. Clay Clay Miner. 46, 586–595.
Schott, J., Oelkers, E.H., 1995. Dissolution and crystallization rates of silicate minerals as a function of chemical affinity. Pure Appl. Chem. 67, 903–910.
Selnert, E., Byegård, J., Widestrand, H., 2008. Forsmark site investigation - Laboratory measurements within the site investigation programme for the transport properties of the rock, Final report (P-07-139). Svensk Kärnbränslehantering AB, Stockholm.
Silva, C.A.R., Liu, X., Millero, F.J., 2002. Solubility of siderite ($FeCO_3$) in NaCl solutions. J. Solut. Chem. 31, 97–108.
SKBF/KBS, 1983. Kärnbränslecykelns slutsteg (vol I-IV). Svensk Kärnbränsleförsörjning AB, Stockholm.
Stumm, W., Morgan, J.J., 1996. Aquatic Chemistry, 3rd Ed. Wiley, New York.
Sugimori, H., Yokoyama, T., Murakami, T., 2009. Kinetics of biotite dissolution and Fe behaviour under low O2 conditions and their implications for Precambrian weathering. Geochim. Cosmochim. Acta 73, 3767–3781.
Taylor, P., Owen, D.G., 1997. Biotite dissolution and oxygen consumption in aqueous media at 100°C (AECL-11571). AECL Whiteshell Laboratories, Pinawa, Manitoba.
Thommes, M., et al., 2015. Physisorption of gases, with special reference to the evaluation of surface area and pore size distribution (IUPAC Technical Report). Pure Appl. Chem. 9–10, 1051–1069.
Turpault, M.P., Trotignon, L., 1994. The dissolution of biotite single crystals in dilute HNO3 at 24C: Evidence of an anisotropic corrosion process of micas in acidic solutions. Geochim. Cosmochim. Acta 58, 2761–2775.
Velbel, M.A., 1985. Geochemical mass balances and weathering rates in forested watersheds of the southern Blue Ridge. Am. J. Sci. 285, 904–930.
White, A.F., Brantley, S.L., 2003. The effect of time on the weathering of silicate minerals: why do weathering rates differ in the laboratory and field? Chem. Geol. 202, 479–506.
White, A.F., Yee, A., 1985. Aqueous oxidation-reduction kinetics associated with coupled electron-cation transfer from iron-containing silicates at 25°C. Geochim. Cosmochim. Acta 49, 1263–1275.
Yu, Q., Kandegedara, A., Xu, Y., Rorabacher, D.B., 1997. Avoiding interferences from Good's buffers: a contiuous series of noncomplexing tertiary amine buffers covering the entire range of pH 3–11. Anal. Biochem. 253, 50–56.